communications biology

Article

https://doi.org/10.1038/s42003-024-07215-0

# Protective role of aconitate decarboxylase 1 in neuroinflammation-induced dysfunctions of the paraventricular thalamus and sleepiness

Check for updates

Jianjun Chang[1], Zijie Li[1], Hui Yuan[2], Xuejiao Wang[1], Jingyi Xu[3], Pingting Yang[3] ✉ & Ling Qin[2] ✉

Sleepiness is commonly associated with neuroinflammation; however, the underlying neuroregulatory mechanisms remain unclear. Previous research suggests that the paraventricular thalamus (PVT) plays a crucial role in regulating sleep-wake dynamics; thus, neurological abnormalities in the PVT may contribute to neuroinflammation-induced sleepiness. To test this hypothesis, we performed electroencephalography recordings in mice treated with lipopolysaccharide (LPS) and found that the mice exhibited temporary sleepiness lasting for 7 days. Using the Fos-TRAP method, fiber photometry recordings, and immunofluorescence staining, we detected temporary PVT neuron hypoactivation and microglia activation from day 1 to day 7 post-LPS treatment. Combining the results of bulk and single-cell RNA sequencing, we found upregulation of aconitate decarboxylase 1 (Acod1) in PVT microglia post-LPS treatment. To investigate the role of Acod1, we manipulated Acod1 gene expression in PVT microglia via stereotactic injection of short hairpin RNA adenovirus. Knockdown of Acod1 exacerbated inflammation, neuronal hypoactivation, and sleepiness. Itaconate is a metabolite synthesized by the enzyme encoded by Acod1. Finally, we confirmed that exogenous administration of an itaconate derivative, 4-octyl itaconate, could inhibit microglia activation, alleviate neuronal dysfunction, and relieve sleepiness. Our findings highlight PVT's role in inflammation-induced sleepiness and suggest Acod1 as a potential therapeutic target for neuroinflammation.

Sleep is a physiological and behavioral process that plays an important role in metabolism and immune system homeostasis. During inflammation, both animals and humans often exhibit sleepiness[1–4]. This is an adaptive central nervous system (CNS) response to help the immune system fight against infection[5]. Sleepiness preserves the energy needed to increase body temperature (fever), which in turn increases the activity of white blood cells and inhibits pathogen growth[6]. Upon recovery from inflammation, the sleepiness disappears; however, the internal mechanism underlying inflammation-induced sleepiness remains unclear.

Previous reports suggested that the sleep-wake rhythm is regulated by multiple subcortical nuclei in the brain, including wake-promoting nuclei such as the paraventricular thalamus (PVT)[7,8], paraventricular hypothalamus (PVH)[9], and basal forebrain (BF)[10]; and sleep-promoting nuclei such as the ventrolateral preoptic nucleus (VLPO)[11]. Because the PVT is located on the midline just ventral to the third ventricle, with an incomplete blood–brain barrier[12–14], it is more vulnerable to inflammatory attacks. PVT neurons are primarily glutamatergic[7] and receive multiple inputs from the brainstem and hypothalamus, projecting to the prefrontal cortex (PFC), nucleus accumbens, and amygdala[8]. PVT neurons display high activity during wakefulness and low activity during sleep[7]. However, the role and potential mechanisms of action of PVT in neuroinflammation-induced sleepiness remain unclear.

PVT also contains some microglia, which are important immune effector cells in the brain[15]. Under systemic inflammatory conditions, inflammatory molecules produced by peripheral immune cells traverse the blood–brain barrier and activate microglia[16]. Previous studies reported that microglia were involved in sleepiness in a mouse model of traumatic brain injury[17]. However, the mechanisms have not yet been fully elucidated. On

[1]Department of Physiology, School of Life Sciences, China Medical University, Shenyang, China. [2]Laboratory of Hearing Research, School of Life Sciences, China Medical University, Shenyang, China. [3]Department of Rheumatology and Immunology, The First Hospital of China Medical University, Shenyang, China.
✉e-mail: yangpingtingting@163.com; qinlingling@yahoo.com

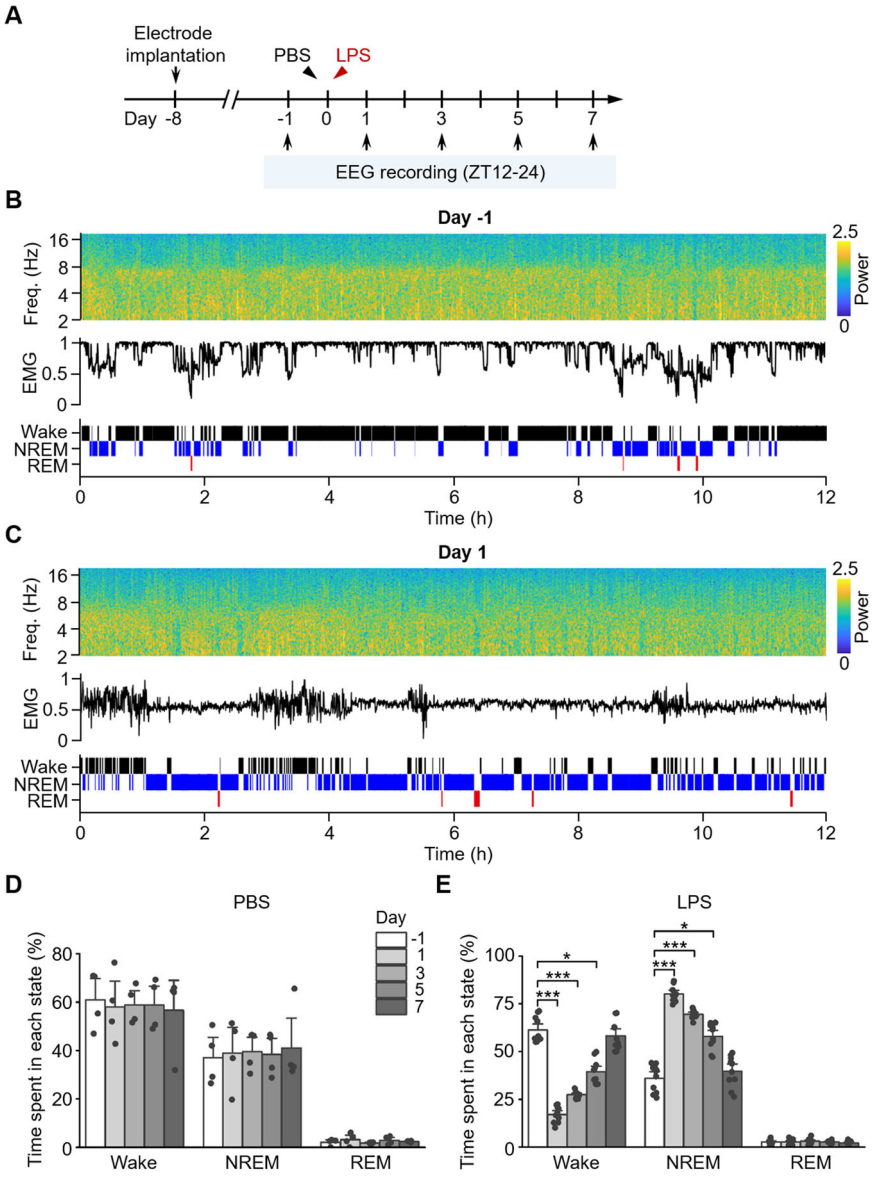


**Fig. 1 | LPS increases NREM period during the active phase. A** Schematic diagram showing the timeline of the experimental protocol. Mice were implanted with electrodes in the prefrontal cortex (PFC) and allowed 7 days for recovery. Electroencephalogram (EEG) recordings were conducted during the active phase [zeitgeber time (ZT) 12-24] 1 day before, 1, 3, 5, and 7 days after the injection of phosphate-buffered saline (PBS)/lipopolysaccharide (LPS). Time-power analysis of PFC EEG, electromyogram (EMG), and hypnogram 1 day before (**B**) and after (**C**) LPS injection. **D** The percentage of time spent in each sleep-wake state at different time points before and after PBS injection. $n = 4$ mice. [Friedman analysis of variance (ANOVA)]. **E** The percentage of time spent in each sleep-wake state at different time points before and after LPS injection. $^{*}P < 0.05$, $^{***}P < 0.001$. $n = 10$ mice. (Friedman ANOVA and One-Way Repeated Measures ANOVA).

the one hand, microglial activation can suppress neuronal activities by releasing cytokines, including interleukin (IL)-1β, IL-6, and tumor necrosis factor-α (TNF-α)[18–20], thereby promoting sleep. On the other hand, the anti-inflammatory process in microglia is simultaneously initiated, limiting release of cytokines, restoring neuronal activity, and ensuring timely termination of sleepiness. Therefore, how the interaction between microglia and neurons contributes to the process of neuroinflammation-induced sleepiness needs to be investigated.

For this purpose, we intraperitoneally injected lipopolysaccharide (LPS) into mice to induce neuroinflammation, and evaluated their sleep-wake states by recording electroencephalograms (EEGs), to reveal the temporal characteristics of sleepiness. We used the immediate early gene Fos-TRAP method and in vivo fiber photometry recording to confirm the correlation between PVT neuronal activity and sleep-wake states. We also performed transcriptome analysis and immunofluorescence staining of brain tissue to explore the pathological changes in PVT, and found an upregulation of aconitate decarboxylase 1 (Acod1) expression in microglia. Itaconate is a metabolite synthesized by the enzyme encoded by Acod1. We further revealed that Acod1 and itaconate had an anti-neuroinflammatory effect and could alleviate sleepiness. Our findings provide valuable insights into the molecular mechanisms regulating the balance between pro- and anti-inflammatory functions in microglia and neuroinflammation-associated sleep-wake alterations.

## Results

### Acute administration of LPS increases the non-rapid eye movement period during the active phase

To investigate the effects of neuroinflammation on sleep, we used a peripherally induced neuroinflammation model by intraperitoneal injection of 1 mg/kg LPS. Control mice received an intraperitoneal injection of phosphate-buffered saline (PBS). The EEG signals were recorded from electrodes implanted in the PFC during the active phase [zeitgeber time (ZT) 12:00–24:00] of the day-night cycle. The EEG recording was conducted 1 day before and 1, 3, 5, and 7 days after PBS/LPS injection (Fig. 1A). Figure 1B, C shows the spectrum of representative EEGs recorded 1 day before and 1 day after LPS injection, respectively. Sleep-wake states were automatically classified into wake, non-rapid eye movement (NREM), and rapid eye movement (REM) sleep according to previously described criteria[21]. LPS injection decreased the wake period and increased the NREM period. Consistent with a previous report[22], normal mice spent a larger proportion of time in the waking state (60.90 ± 5.91%) than in NREM sleep (37.02 ± 5.63%) during the active phase. In contrast, the duration of REM

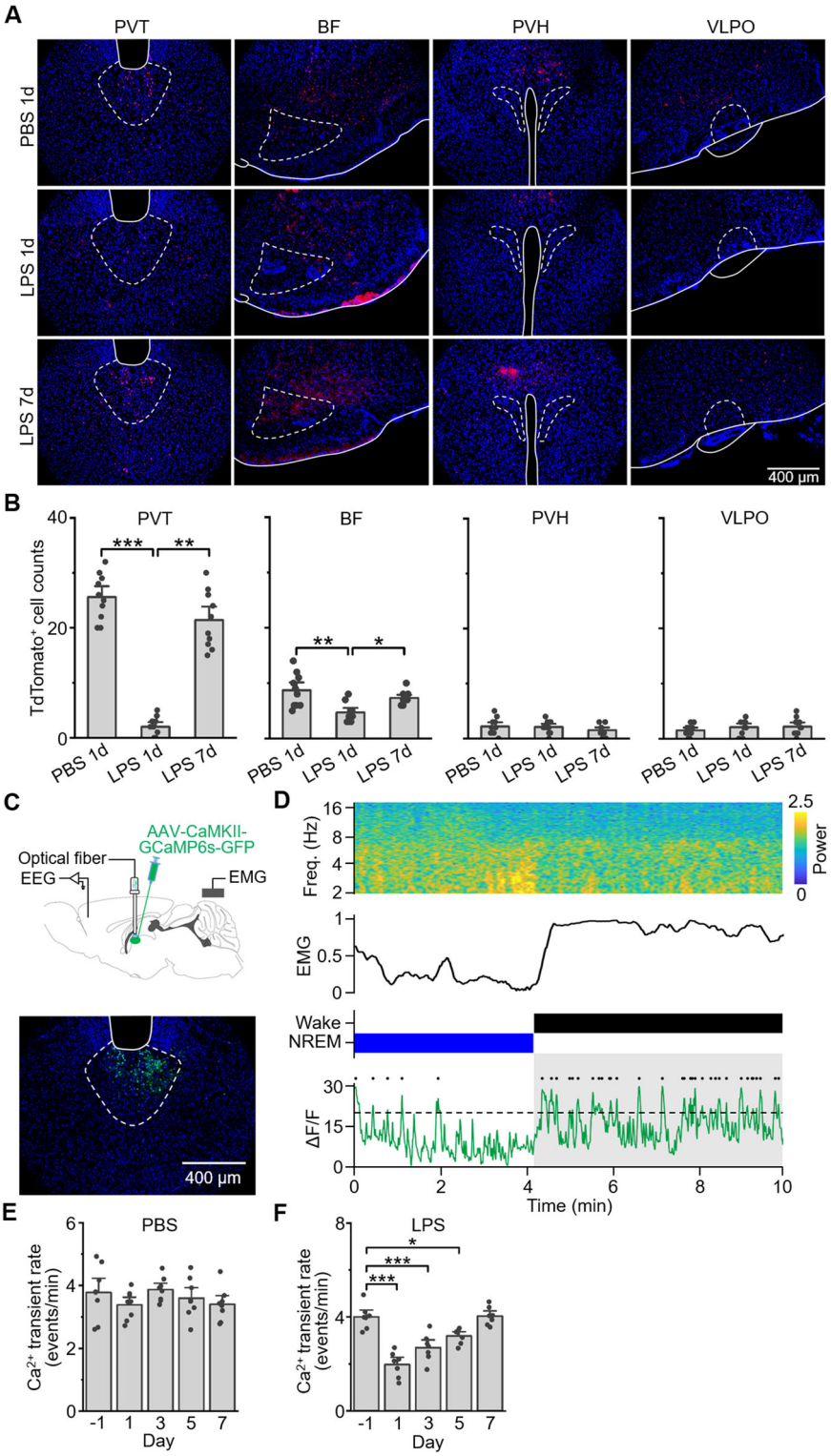


**Fig. 2 | LPS-induced reduction in neuronal activity in the paraventricular thalamus. A** Representative micrographs of FOS expression (TdTomato, red) and DAPI staining (blue) in the paraventricular thalamus (PVT), basal forebrain (BF), paraventricular hypothalamus (PVH), and ventrolateral preoptic nucleus (VLPO) on day 1 after PBS/LPS injection, as well as day 7 after LPS injection. **B** Quantitative analysis on TdTomato$^+$ cells in different brain regions under different treatment conditions. $^*P < 0.05$, $^{**}P < 0.01$, $^{***}P < 0.001$. $n = 10$ mice. (Kruskal-Wallis ANOVA and One-Way ANOVA). **C** Top: schematic diagram depicting virus injection, fiber photometry recording of population $Ca^{2+}$ activity of glutamatergic neurons, recordings of EEG and EMG during the active phase in moving mice. Bottom: Image showing the expression of GCaMP6s-GFP (green) and DAPI staining (blue) in the PVT. **D** The EEG spectrogram, EMG, hypnogram, and fiber photometry trace of a normal mouse. Dot marks a transient event higher than mean + standard deviation of ΔF/F0. **E**, **F** Rate of $Ca^{2+}$ transient events during the active phase 1 day before, 1, 3, 5, and 7 days after the injection of PBS (E)/LPS (**F**). $^*P < 0.05$, $^{***}P < 0.001$. $n = 7$-8 mice. (One-Way Repeated Measures ANOVA).

sleep (2.07 ± 0.70%) was very short (Fig. 1D). Moreover, PBS injection had no significant effect on the relative proportions of the sleep-wake states in mice. LPS injection caused a large reduction of the wake period on day 1, followed by a gradual rebound from day 3 and almost completely recovery by day 7 (Fig. 1E). The NREM period was accordingly increased on day 1, and gradually returned to the baseline level by day 7. In contrast, the REM period did not significantly change. These results suggested that acute administration of LPS induced temporary sleepiness lasting for approximately 7 days.

### Neuronal activity in the PVT is reduced by LPS injection

We used double transgenic TRAP2;Ai14 mice, in which active neurons express the fluorescent protein TdTomato, to examine the effect of LPS injection on neuronal activities in sleep-wake regulating nuclei: PVT, BF, PVH, and VLPO. A large number of TdTomato$^+$ cells were observed in the PVT of PBS-injected mice during the active phase, but they almost completely disappeared on day 1 after LPS injection, and reappeared on day 7 (Fig. 2A). A similar phenomenon occurred in the BF. PBS-injected mice exhibited few TdTomato$^+$ cells in the PVH or VLPO, and LPS injection had

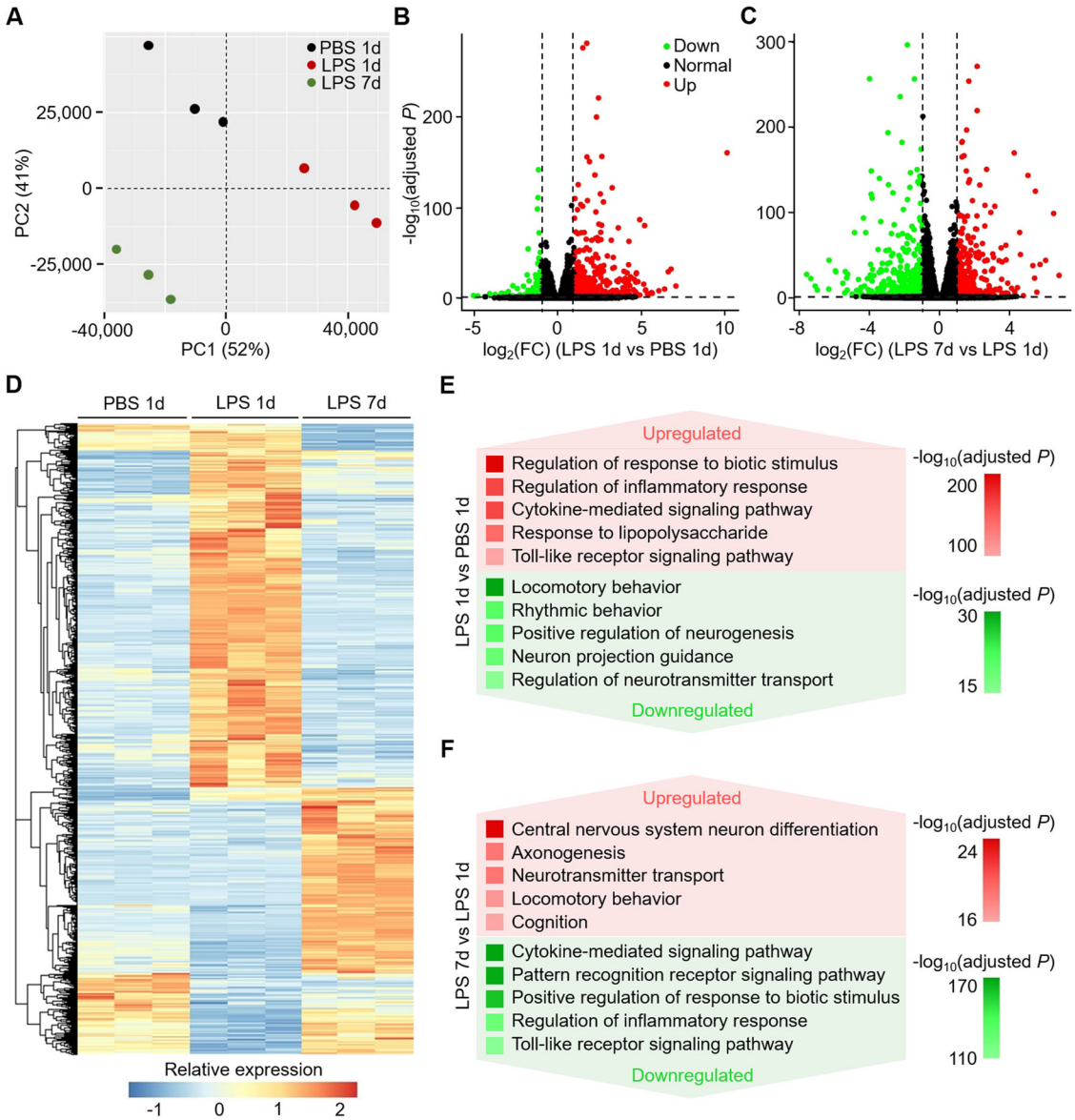


**Fig. 3 | Bulk RNA sequencing analysis of PVT in response to PBS and LPS treatment. A** Principal component analysis based on overall gene expression across all samples. Volcano plots displaying differentially expressed genes (DEGs) between LPS 1 d and PBS 1 d groups (**B**), as well as LPS 7 d and LPS 1 d groups (**C**). **D** Hierarchical clustering analysis of all DEGs. The top 5 Gene Ontology (GO) biological processes (BPs) terms of upregulated and downregulated DEGs between LPS 1 d and PBS 1 d groups (**E**), as well as LPS 7 d and LPS 1 d groups (**F**).

no significant effect. Quantitative statistics of TdTomato$^+$ cell counts confirmed the above observations (Fig. 2B). We next injected adenovirus-associated virus (AAV)-CaMKII-GCaMP6 into the PVT and examined neuronal activity of behaving mice through fiber photometry recording (Fig. 2C). Consistent with previous reports[7], the rate of $Ca^{2+}$ transient during the wake period was higher than that during NREM sleep (Fig. 2D). Therefore, the higher $Ca^{2+}$ transient rate is; the longer wake period is. In contrast, the lower $Ca^{2+}$ transient rate is; the longer NREM period is. We found that the mean rate of $Ca^{2+}$ transient during the active phase was temporarily decreased by LPS injection but unaffected by PBS injection (Fig. 2E, F). Thus, LPS injection-induced sleepiness may be associated with a reduction of $Ca^{2+}$ transient rate in the PVT.

### Transcriptome changes in the PVT induced by LPS injection

Next, we evaluated LPS-induced transcriptome changes in the PVT using bulk RNA sequencing (RNA-seq) analysis of mice 1 day after PBS/LPS injection or 7 days after LPS injection. Principal component analysis (PCA) analysis based on overall gene expression separated the three groups into distinct clusters (Fig. 3A). A total of 604 differentially expressed genes (DEGs) were identified in the LPS 1 d group compared with the PBS 1 d group, with 491 upregulated and 113 downregulated genes (Fig. 3B). Furthermore, in the LPS 7 d group, a total of 961 DEGs were identified compared with the LPS 1 d group, with 420 upregulated and 541 downregulated genes (Fig. 3C). Hierarchical clustering analysis of all DEGs also demonstrated marked transcriptome differences among the three groups, consistent with the results shown in Fig. 3A (Fig. 3D). Gene Ontology (GO) enrichment analysis revealed that the upregulated DEGs between the LPS 1 d and PBS 1 d groups were predominantly enriched in biological processes (BPs) associated with inflammatory pathways. Conversely, the downregulated DEGs were primarily enriched in BPs related to locomotion, rhythm, and neuron-related processes (Fig. 3E). Furthermore, when analyzing the DEGs between the LPS 7 d and LPS 1 d groups, the GO enrichment analysis demonstrated that the upregulated BPs were associated with neuron-related processes, locomotion, and cognition, while the downregulated BPs were associated with inflammatory pathways (Fig. 3F). Thus, the transcriptome changes in the LPS 1 d group were completely reversed in LPS 7 d group.

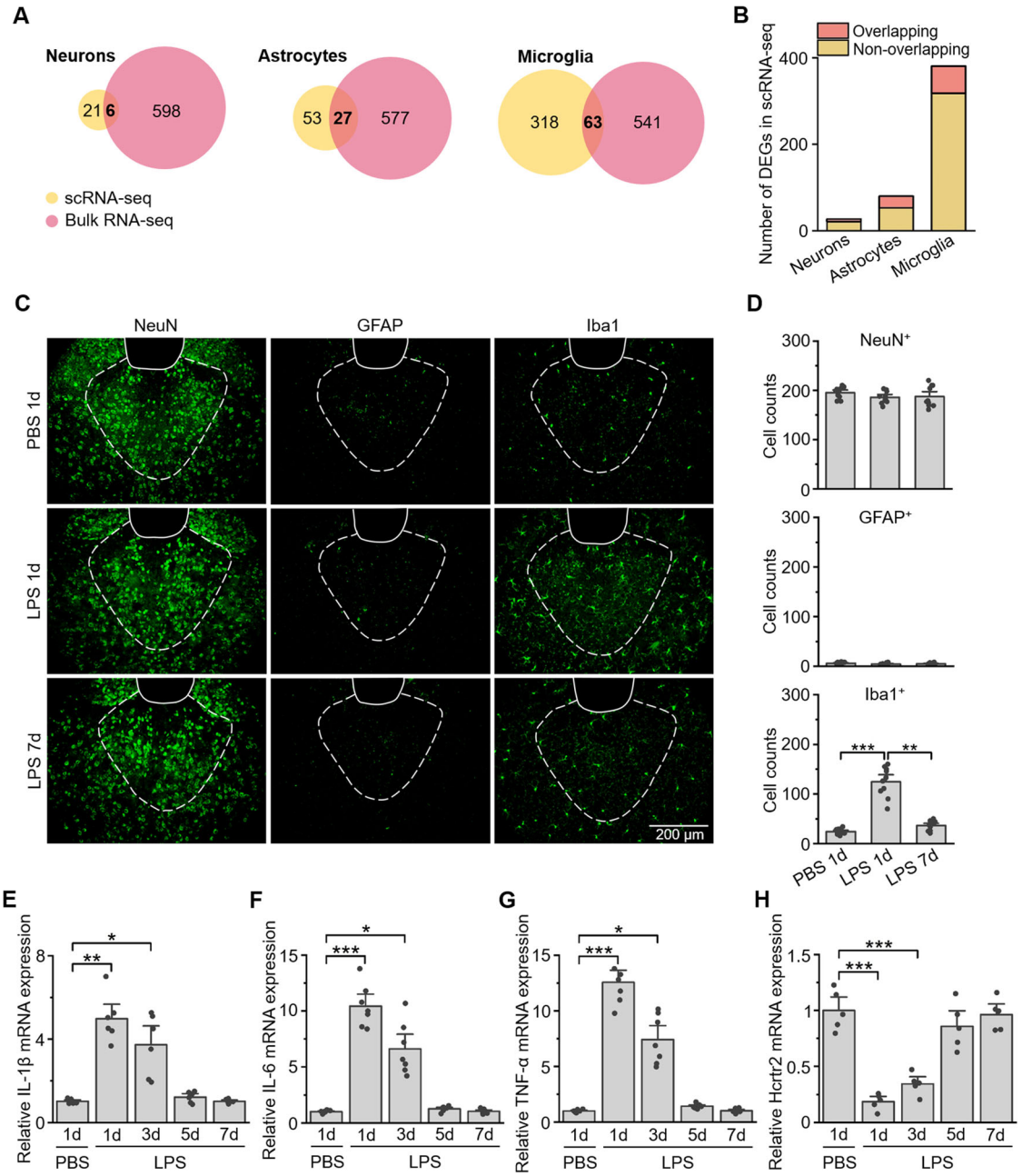


**Fig. 4 | LPS activates microglia in the PVT. A** The overlapping between DEGs identified through bulk RNA-seq and those detected in neurons, astrocytes, or microglia from a published scRNA-seq dataset (GSE112436). **B** The number of overlapping and non-overlapping DEGs between bulk RNA-seq and scRNA-seq dataset. **C** Representative microphotographs showing NeuN, GFAP, and Iba1-immunopositive cells in the PVT on day 1 after PBS/LPS injection and day 7 after LPS injection. A white dotted line outlines the PVT region. **D** Quantitative analysis of NeuN$^+$, GFAP$^+$, and Iba1$^+$ cells. $^{**}P < 0.01$, $^{***}P < 0.001$. $n = 10$ mice. (Kruskal-Wallis ANOVA and One-Way ANOVA). (E–H) Relative mRNA expression of IL-1β, IL-6, TNF-α and Hcrtr2 in the PVT under different treatment conditions. $^{*}P < 0.05$, $^{**}P < 0.01$, $^{***}P < 0.001$. $n = 5$-7 mice. (Kruskal-Wallis ANOVA and One-Way ANOVA).

### LPS injection induced microglial activation in the PVT

In addition to our own analysis, we examined a publicly available single-cell RNA sequencing (scRNA-seq) dataset (GSE112436) of mouse brains subjected to acute LPS treatment[23]. By specifically identifying LPS-induced DEGs in neurons, astrocytes, and microglia, we observed that microglia exhibited the highest number of DEGs. Moreover, there was the greatest overlap between the DEGs identified in our bulk RNA-seq and those identified specifically in microglia in the scRNA-seq dataset (Fig. 4A, B). These findings indicated that the transcriptome changes induced by LPS were pronounced in microglia.

To validate above findings, we performed immunofluorescence staining of brain slices of the PVT and analyzed the density and morphology of cells expressing specific neuronal (NeuN), astrocytic (GFAP), and microglial (Iba1) markers (Fig. 4C). Remarkably, the densities and morphologies of neurons were similar among all three experimental groups. Astrocytes in the PVT were relatively scarce in all three groups. However, microglia density exhibited a significant increase on day 1 after LPS injection, subsequently returned to baseline levels by day 7 (Fig. 4C, D).

We utilized quantitative polymerase chain reaction (qPCR) to detect the expression levels of pro-inflammatory cytokines, including *IL-1β*, *IL-6*,

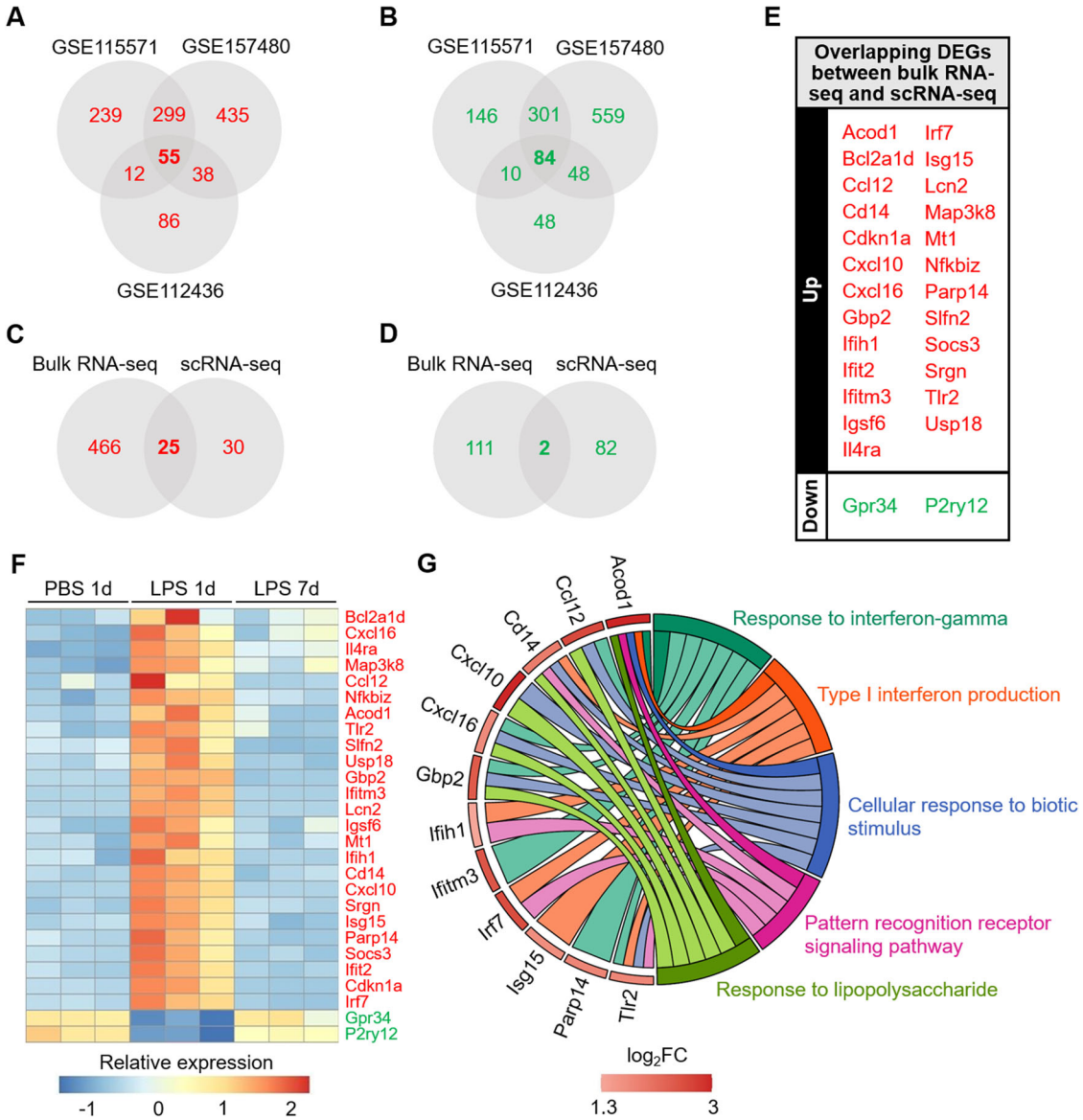


**Fig. 5 | LPS-induced DEGs in the microglia.** Venn diagrams of upregulated (**A**) and downregulated (**B**) DEGs from 3 published microglial scRNA-seq datasets. Venn diagrams of upregulated (**C**) and downregulated (**D**) DEGs between bulk RNA-seq and microglial scRNA-seq datasets. **E** Names of the overlapping DEGs. **F** Gene expression heatmap conducted on bulk RNA-seq data showing the relative expression levels of the overlapping DEGs. **G** Chord plot depicting the relationship between the overlapping DEGs and GO BPs. The top 5 BPs are presented.

and *TNF-α*, in the PVT. Our results indicated a substantial increase in the expression of these pro-inflammatory cytokines on day 1 after LPS injection, followed by a gradual decline from day 3, eventually culminating in near-complete recovery by day 5 (Fig. 4E–G). TNF-α has been documented to suppress the expression of the orexin receptor 2 (OX2R)[24], a specific target for orexin ligands[25,26]. Previous research has demonstrated that OX2R knockout mice exhibit narcolepsy-like phenotypes, and the administration of an OX2R agonist can enhance wakefulness[27–29]. We also found a pronounced reduction in mRNA expression of the *Hcrtr2* gene, encoding the OX2R, in the PVT on day 1 after LPS injection. This decrease gradually recovered from day 3, with near-complete restoration of expression levels by day 7 (Fig. 4H).

### LPS-induced DEGs in the microglia

We downloaded three scRNA-seq datasets (GSE115571, GSE157480, and GSE112436) from the Gene Expression Omnibus repository[23,30,31] and identified LPS-induced DEGs in microglia within each dataset. Interestingly, all three datasets shared a common set of 55 upregulated DEGs and 84 downregulated DEGs (Fig. 5A, B). There were 25 upregulated DEGs and 2 downregulated DEGs in our bulk RNA-seq data overlapping with the DEGs shared across the scRNA-seq datasets (Fig. 5C, D). These overlapping upregulated DEGs, including *Acod1*, *Ccl12*, *Cd14*, *Cxcl10*, and *Cxcl16*, are primarily associated with inflammatory responses. Similarly, the downregulated DEGs *Gpr34* and *P2ry12*, derived from the P2Y-related receptor family, are also known to mediate inflammatory responses[32,33] (Fig. 5E).

To visualize the expression patterns of the overlapping DEGs, a gene expression heatmap was generated using our bulk RNA-seq data. The expression levels of these DEGs exhibited significant changes 1 day after LPS injection and largely returned to baseline levels by 7 days (Fig. 5F). Additionally, a chord plot was generated to illustrate the relationship between the overlapping DEGs and GO terms associated with the top five BPs: response to interferon-gamma, type I interferon production, cellular response to biotic stimulus, pattern recognition receptor signaling pathway, and response to LPS (Fig. 5G). These BPs were primarily involved in cytokine-mediated inflammatory responses. Remarkably, *Acod1* participated in all five BPs, suggesting that it plays a key role in LPS-induced inflammatory responses.

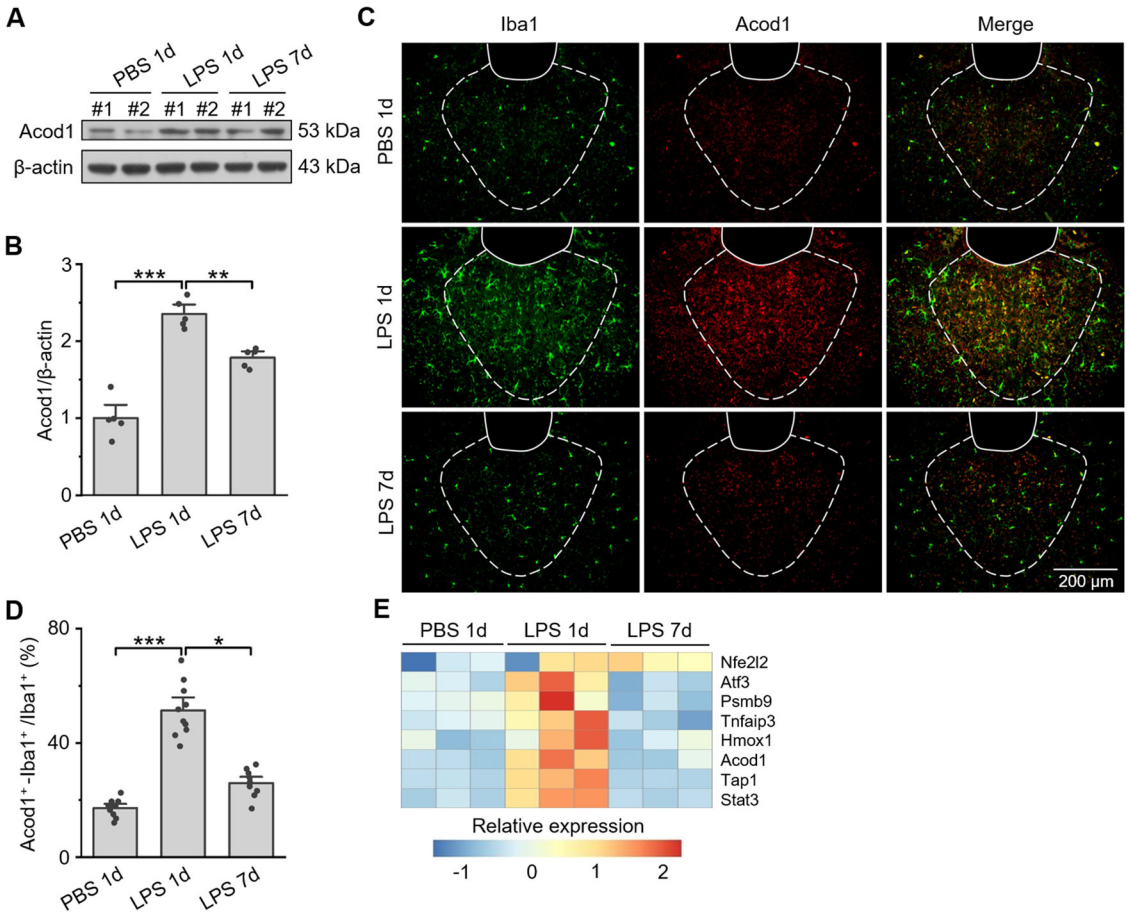


**Fig. 6 | LPS-induced expression of aconitate decarboxylase 1 in PVT microglia.** **A** Representative western blot images of aconitate decarboxylase 1 (Acod1) and β-actin protein expression in the PVT on day 1 after PBS/LPS injection and day 7 after LPS injection. **B** Quantitative analysis of Acod1 protein expression normalized to β-actin. $^{**}P < 0.01$, $^{***}P < 0.001$. $n = 5$ mice. (One-Way ANOVA). **C** Representative microphotographs showing Iba1 and Acod1-immunopositive cells in the PVT under different treatment conditions, with a white dotted line outlining the PVT region. **D** Quantitative analysis of Iba1$^+$-Acod1$^+$ cells in the PVT. $^{*}P < 0.05$, $^{***}P < 0.001$. $n = 10$ mice. (Kruskal-Wallis ANOVA). **E** Gene expression heatmap showing relative expression level of Acod1 and its downstream genes in the bulk RNA-seq.

### Acod1 induction in PVT microglia of LPS-treated mice

Western blot analysis confirmed that the protein expression of Acod1 was upregulated on day 1 after LPS injection and returned to the baseline level by 7 days (Fig. 6A, B). Immunofluorescence staining of brain slices showed that the expression of Acod1 was low in the PVT microglia of PBS 1 d mice, but significantly increased in activated microglia of LPS 1 d mice and largely disappeared in LPS 7 d mice (Fig. 6C, D). In addition, we observed relative weak expression of Acod1 outside of the PVT. In this study, we administered a low dose of LPS, which was insufficient to induce complete disruption of the blood-brain barrier[34,35]. The subsequent inflammatory response within the brain was relatively localized, predominantly observed in the PVT. In alignment with this spatially restricted inflammatory response, the expression of Acod1 exhibited a correspondingly circumscribed pattern. These results confirmed an association between Acod1 and the activation of microglia. Our bulk RNA-seq data also showed that the mRNA levels of downstream genes of Acod1 were upregulated together with Acod1 on day 1 after LPS injection and returned to the baseline level by 7 days (Fig. 6E).

### Knockdown of Acod1 in the PVT microglia exacerbates LPS-induced abnormalities

We conducted a knockdown of Acod1 in the PVT microglia of mice to investigate the role of Acod1 in the neuroinflammation and sleepiness induced by LPS (Fig. 7A). To achieve this, we synthesized AAV-Cx3cr1-Acod1-short hairpin RNA (shRNA)-GFP (Cx3cr1-shAcod1) and its control AAV-Cx3cr1-shRNA-GFP (Cx3cr1-shRNA). We then assessed the transfection efficiency of Cx3cr1-shRNA and Cx3cr1-shAcod1 in neurons, astrocytes and microglia within the PVT of mice. The transfection efficiency of Cx3cr1-shRNA and Cx3cr1-shAcod1 was 0% in neurons (Supplementary Fig. 1A, B) and astrocytes (Supplementary Fig. 1C, D), but about 60% in microglia (Supplementary Fig. 1E, F).

Transfection with Cx3cr1-shAcod1 effectively suppressed the expression of Acod1 in the PVT after LPS injection (Fig. 7B, C). The qPCR results of the PVT brain tissues showed that both LPS injection and Acod1 knockdown significantly elevated the levels of *IL-1β* (Fig. 7D). There was a significant interaction between LPS injection and Acod1 knockdown. On days 1 and 7 after LPS injection, the Acod1 knockdown groups exhibited sustained upregulation of *IL-1β* levels (Fig. 7D), which were significantly higher than those in the virus control groups. Similar trends were observed in the levels of *IL-6* and *TNF-α* (Fig. 7E, F). It can be seen that Acod1 knockdown extended the duration of the inflammatory response induced by LPS.

Using TRAP2;Ai14 mice, we assessed neuronal activities in the PVT. In the virus control group, the number of TdTomato$^+$ cells was significantly decreased on day 1 after LPS injection and showed recovery on day 7; however, the Acod1 knockdown group displayed a continuous decline in the number of TdTomato$^+$ cells in the PVT after LPS injection, which was not restored on day 7 (Fig. 7G). Concurrently, on both days 1 and 7 after LPS injection, the experimental groups exhibited longer NREM periods compared with the control groups (Fig. 7H). On the basis of these findings,

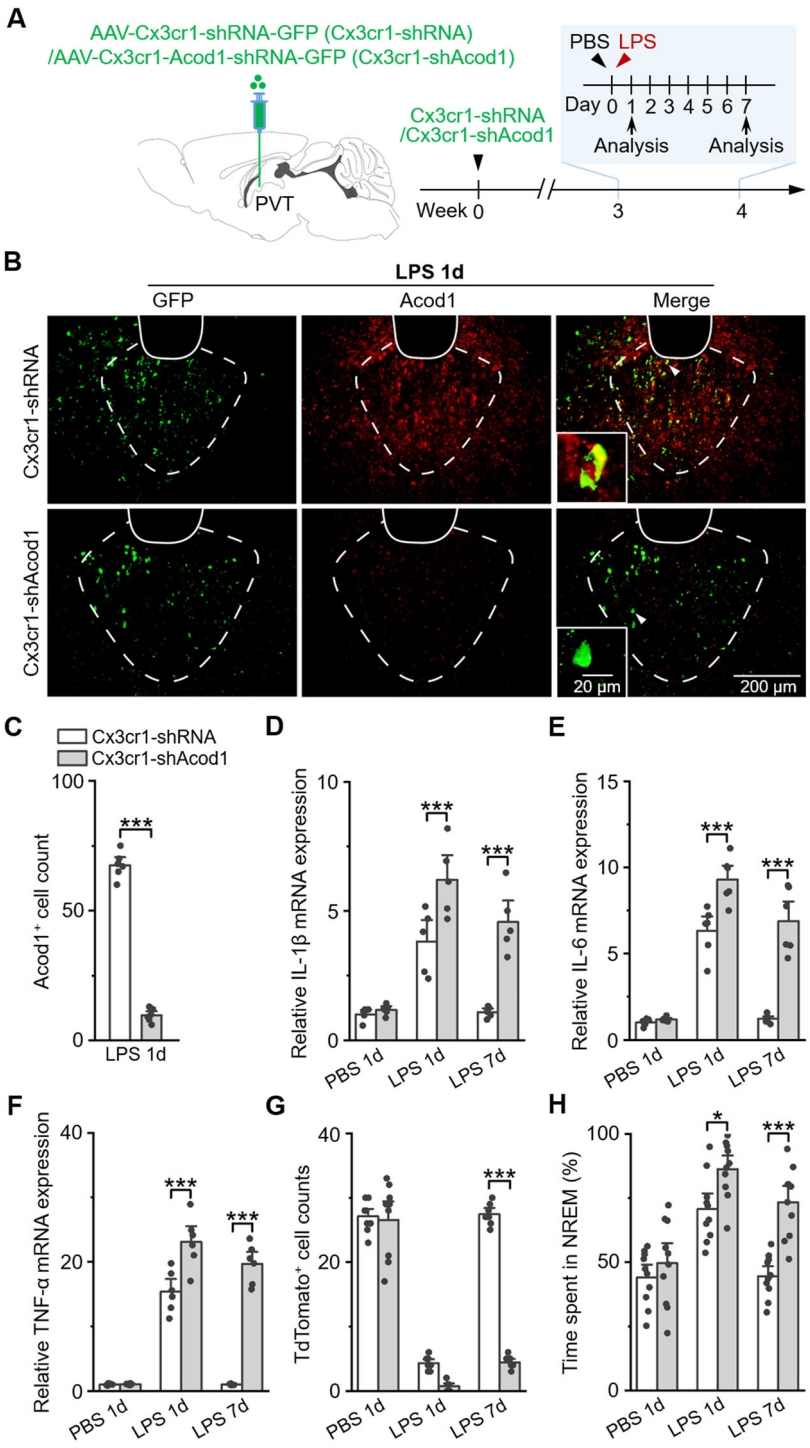


**Fig. 7 | Knockdown of Acod1 in the PVT microglia aggravates abnormalities induced by LPS.** (A) Schematic diagram showing the timeline of Acod1 knockdown and LPS administration. (B) Fluorescent expression of adeno-associated virus (GFP, green) and Acod1 in the PVT of mice injected with AAV-Cx3cr1-shRNA-GFP (Cx3cr1-shRNA) or AAV-Cx3cr1-Acod1-shRNA-GFP (Cx3cr1-shAcod1) 1 day after LPS administration. (C) Quantitative analysis of Acod1$^+$ cells in the PVT 1 day after LPS administration. $^{***}P < 0.001$. $n = 6$ mice. Unpaired Student's two-tailed t-test). (D–F) Relative mRNA expression of pro-inflammatory cytokines in the PVT in mice treated with Cx3cr1-shRNA or Cx3cr1-shAcod1, on day 1 after PBS/LPS injection and day 7 after LPS injection. $^{***}P < 0.001$. $n = 5$-6 mice. (Two-Way ANOVA). (G) Quantitative analysis on TdTomato$^+$ cells in the PVT of TRAP2;Ai14 mice under different treatment conditions. $^{***}P < 0.001$. $n = 7$-9 mice. (Two-Way ANOVA). (H) The percentage of time spent in NREM period under different treatment conditions. $^{*}P < 0.05$, $^{***}P < 0.001$. $n = 10$ mice. (Two-Way Repeated Measures ANOVA).

Acod1 knockdown clearly led to a prolonged reduction in neuronal activity in the PVT, which consequently exacerbated sleepiness.

### Administration of 4-octyl itaconate ameliorates LPS-induced PVT abnormalities and sleepiness

Itaconate is a metabolite synthesized by the enzyme encoded by Acod1 (Fig. 8A), and therefore we next investigated the potential impact of its derivative, 4-octyl itaconate (4-OI), on neurological abnormalities and sleepiness induced by LPS. Mice were intraperitoneally administered 25 mg/kg of 4-OI, with doses given 2 h before, 12 h after, and 24 h after LPS injection (Fig. 8B). Administration of 4-OI significantly ameliorated the activation of PVT microglia (Fig. 8C, D). The administration of 4-OI reduced the levels of the pro-inflammatory cytokines *IL-1β* (Fig. 8E), *IL-6* (Fig. 8F) and *TNF-α* (Fig. 8G) in the PVT. Furthermore, 4-OI administration restored the rate of $Ca^{2+}$ transient (Fig. 8H), and shortened the NREM period (Fig. 8I). These findings indicate a potential therapeutic effect of 4-OI on neuroinflammation-induced sleepiness.

### Itaconate suppresses microglial activation via modulation of the Keap1/Nrf2/HO-1/HIF-1α pathway

Previous studies on macrophages have found that Acod1 catalyzes the decarboxylation of cis-aconitate, leading to elevated itaconate levels.

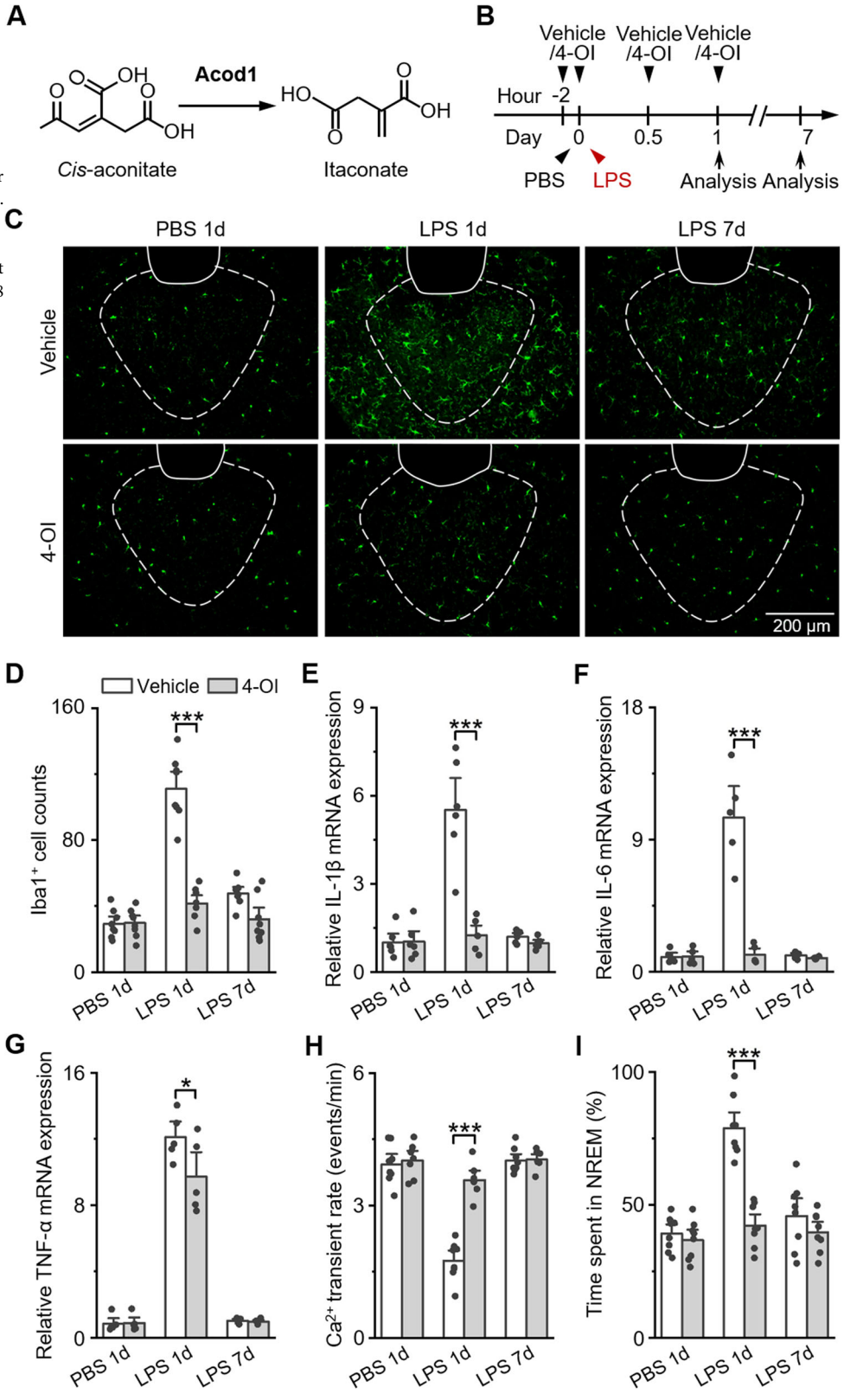


**Fig. 8 | Administration of 4-octyl itaconate ameliorates LPS-induced PVT abnormalities and sleepiness. A** Itaconate synthesis process. **B** Schematic diagram showing the timeline of the administration of 4-octyl itaconate (4-OI). **C** Representative microphotographs showing Iba1 expression in the PVT in vehicle or 4-OI-treated mice 1 day after PBS/LPS injection and 7 days after LPS injection. **D** Quantitative analysis on Iba1$^+$ cells. $^{***}P < 0.001$. $n = 8$ mice. (Two-Way ANOVA). **E–G** Relative mRNA expression of pro-inflammatory cytokines in the PVT under different treatment conditions. $^{*}P < 0.05$, $^{***}P < 0.001$. $n = 6$-8 mice. (Two-Way ANOVA). H Rate of calcium transient events under different treatment conditions. $^{***}P < 0.001$. $n = 7$-8 mice. (Two-Way Repeated Measures ANOVA). **I** The percentage of time spent in NREM period under different treatment conditions. $^{***}P < 0.001$. $n = 10$ mice. (Two-Way Repeated Measures ANOVA).

Itaconate subsequently modifies and inhibits Kelch-like ECH-associated protein 1 (Keap1) through a specific cysteine modification termed dicarboxypropylation[36]. This modification promotes the dissociation of nuclear factor erythroid 2-related factor 2 (Nrf2) from the Keap1-Nrf2 complex, allowing Nrf2 to activate gene transcription such as Heme oxygenase 1 (HO-1)[36]. As an antioxidant enzyme, HO-1 mitigates reactive oxygen species (ROS) accumulation, thereby inhibits the activity of HIF-1α and the transcription of pro-inflammatory cytokine IL-1β[37,38]. Nrf2 can also directly suppresses IL-1β gene transcription (Fig. 9A).

To confirm a similar molecular mechanisms underlying Acod1's anti-inflammatory effects in microglia, we employed western blot analysis to assess protein expression levels across the Keap1/Nrf2/HO-1/

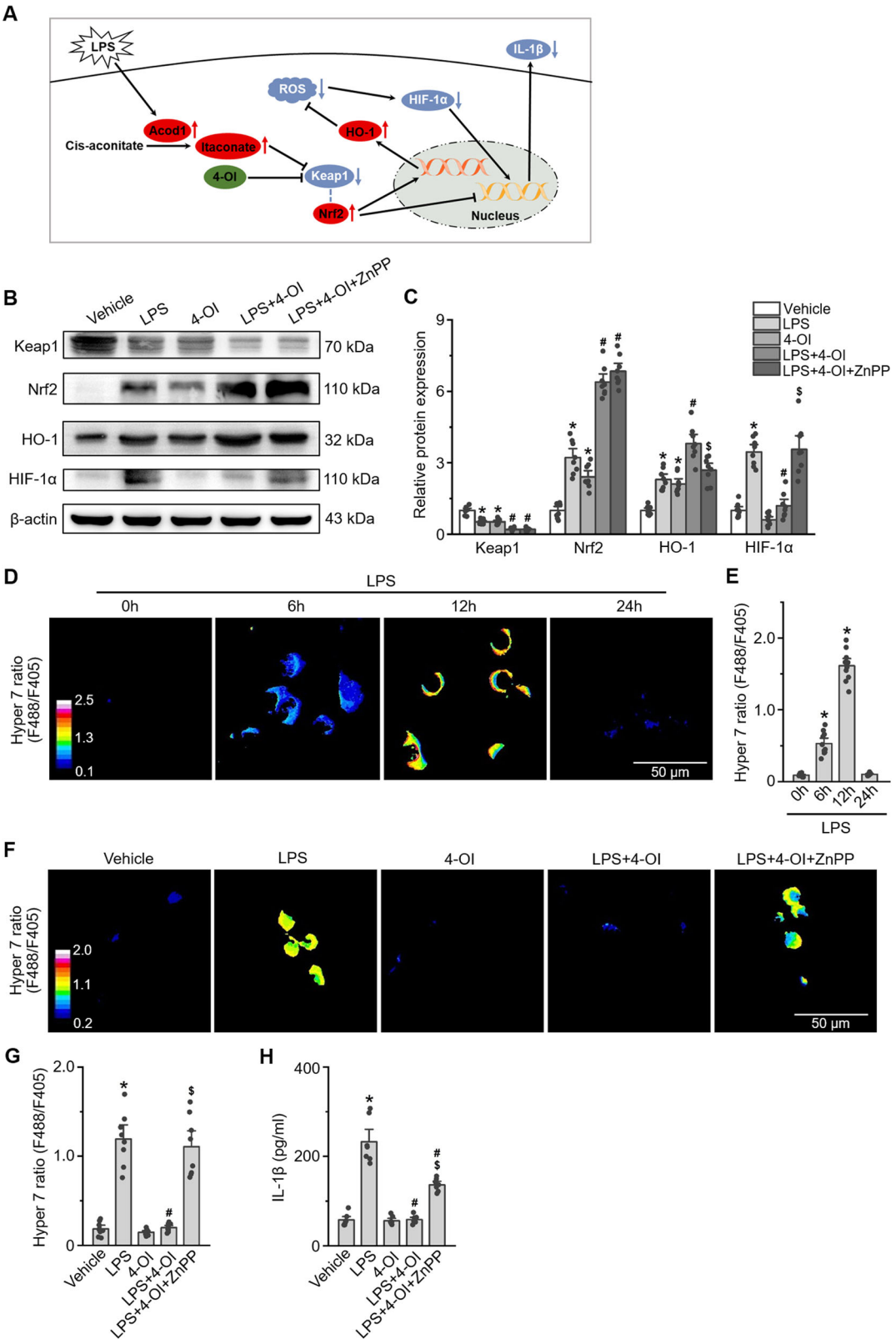


HIF-1α signaling axis in BV2 microglia. As shown in Fig. 9B, C, LPS treatment led to a significant decrease in Keap1 protein levels and an increase in Nrf2, HO-1, and HIF-1α expression at 12 hours (Fig. 9B, lane 2 vs lane 1). Treatment with 4-OI also resulted in decreased Keap1 expression and increased expression of Nrf2 and HO-1, but did not significantly affect HIF-1α expression (Fig. 9B lane 3 vs lane 1 and Fig. 9C). Pretreatment with 4-OI prior to LPS exposure further reduced Keap1 expression and enhanced Nrf2 and HO-1 expression, while also significantly attenuating HIF-1α expression (Fig. 9B lane 4 vs lane 2 and Fig. 9C). The HO-1 inhibitor zinc protoporphyria (ZnPP) partially reversed the 4-OI-induced increase in HO-1 expression and restored HIF-1α levels in LPS-stimulated BV2 cells, although it did not

**Fig. 9 | Itaconate suppresses microglial activation through the modulation of the Keap1/Nrf2/HO-1/HIF-1α signaling pathway. A** A schematic diagram illustrating the mechanism by which Acod1 modulates the Keap1/Nrf2/HO-1/HIF-1α pathway, thereby inhibiting the transcription of the IL-1β gene. **B** Representative western blot images displaying the protein expression levels of Keap1, Nrf2, HO-1, HIF-1α, and β-actin in BV2 cells. **C** Quantitative analysis of protein expression levels normalized to β-actin. $^{*}P < 0.001$ vs vehicle group, $^{\#}P < 0.001$ vs LPS group, $^{\$}P < 0.001$ vs LPS + 4-OI group. $n = 8$ samples. (One-Way ANOVA). **D** False color ratio images of Hyper 7 fluorescence in BV2 cells, calculated from the fluorescence intensity at 488 and 405 nm excitation wavelengths, at 6, 12, and 24 hours following stimulation with 1 μg/mL LPS. **E** Quantitative analysis of the Hyper 7 ratio in BV2 cells. $^{*}P < 0.001$ vs 0 h group. $n = 10$ samples. (One-Way ANOVA). **F** False color ratio images of Hyper 7 fluorescence in BV2 cells. **G** Quantitative analysis of the Hyper 7 ratio in BV2 cells. $^{*}P < 0.001$ vs vehicle group, $^{\#}P < 0.001$ vs LPS group, $^{\$}P < 0.001$ vs LPS + 4-OI group. $n = 8$ samples. (One-Way ANOVA). **H** Measurement of IL-1β levels in the supernatant of BV2 cell cultures. $^{*}P < 0.001$ vs vehicle group, $^{\#}P < 0.001$ vs LPS group, $^{\$}P < 0.001$ vs LPS + 4-OI group. $n = 7$ samples. (One-Way ANOVA).

significantly alter the effects of 4-OI on the expression of Keap1 and Nrf2 in LPS-treated cells (Fig. 9B lane 5 vs lane 4 and Fig. 9C).

To monitor the changes in reactive oxygen species levels in microglia following LPS stimulation and evaluate the antagonistic effects of 4-OI on these changes, we transfected BV2 microglial cells with a mitochondria-targeted Hyper7 construct, an ultrasensitive genetically encoded $H_2O_2$ biosensor[39]. The HyPer7 signal in the cells exposed to 1 μg/mL LPS was quantified by the $F_{488}$ to $F_{405}$ fluorescence intensity ratio. The level of $H_2O_2$ exhibited a significant increase at the 6-hour time point post-LPS exposure, peaking at 12 hours, and subsequently returning to baseline levels by 24 hours (Fig. 9D, E).

In BV2 cells expressing HyPer7 and treated with LPS for 12 hours, 4-OI induced a significant decrease in the level of $H_2O_2$. Notably, ZnPP almost completely blocked the therapeutic effect of 4-OI on the level of $H_2O_2$ (Fig. 9F, G). ELISA assay was utilized to quantify IL-1β levels in the culture supernatant of BV2 cells. LPS treatment significantly increased IL-1β levels, which was inhibited by 4-OI. Furthermore, ZnPP partially weakened the inhibitory effect of 4-OI on IL-1β levels (Fig. 9H). These findings indicate that itaconate suppresses microglial activation by modulating the Keap1/Nrf2/HO-1/HIF-1α pathway, leading to decreased mitochondrial $H_2O_2$ production, reduced level of pro-inflammatory cytokines.

## Discussion

Inflammation often induces temporary sleepiness in both animals and humans[40,41]. The main objective of this study was to elucidate the neuroregulatory mechanisms underlying inflammation-induced sleepiness. We first confirmed that LPS injection could induce temporary sleepiness lasting for approximately 7 days in mice. Subsequently, using the Fos-TRAP method and in vivo fiber photometry recordings, we found temporary hypoactivation of the PVT neurons from day 1 to day 7 after LPS injection. Transcriptome analysis revealed that LPS injection upregulated the expression of genes associated with inflammatory pathways and downregulated the expression of genes related to locomotion, rhythm, and neuron-related processes. The transcriptome changes were more pronounced in the microglia, which were temporally activated by LPS injection. Furthermore, we found that Acod1 exerts an anti-inflammatory effect in microglia to maintain homeostasis of neuronal activity and the sleep-wake cycle. Finally, we confirmed that exogenous administration of an itaconate derivative, 4-OI, could also suppress the inflammatory response of microglia, alleviate PVT hypoactivation, and mitigate sleepiness. Our findings provide valuable insights into the mechanisms underlying inflammation-induced sleepiness and the role of Acod1 in balancing pro- and anti-inflammatory processes in microglia.

During sepsis episodes, individuals often experience sickness behavior, including reduced motor activity, shivering, temperature instability, and sleepiness[42,43]. LPS has been widely used to induce sepsis in laboratory animals[44–46]. A previous study demonstrated that mice treated with a standard intraperitoneal dose of LPS at 1 mg/kg survived a 3-day testing period[47]. Moreover, similar doses of LPS have been found to significantly upregulate CNS cytokines and induce evident sickness behavior in mice at 24 h[48,49]. Conversely, intraperitoneal administration of 5–10 mg/kg LPS resulted in mortality rates of 75–90% within 3 days in mice[50,51]. Thus, an LPS dose of 1 mg/kg was deemed appropriate and safe for subsequent experiments. According to previous reports, the dose of LPS used in this study is not sufficient to cause complete damage to the BBB[34,35]. However, LPS treatment can increase the adhesion and rolling probabilities of inflammatory cells in peripheral blood, such as macrophages[52,53]. This enhancement in cellular dynamics promotes a vigorous interaction between macrophages and vascular endothelial cells, thereby initiating a cascade of inflammatory signaling pathways[54,55]. Consequently, this sequence of events culminates in the microglial activation.

Previous studies have mainly focused on the onset of sleepiness induced by LPS rather than its resolution. The present study revealed that 1 mg/kg LPS-induced sleepiness was most serious at 24 h, gradually recovered thereafter, and usually recovered fully after approximately 7 days. During the acute phase of inflammation, sleepiness helps protect neurological function by reducing the energy consumption of neurons. Although neuroinflammation is initially a neuroprotective mechanism against injuries or infection, sustained neuroinflammation and long-term suppression of neuronal activity can induce neurotoxicity and permanent functional impairment[56]. Hence, maintaining a dynamic balance between pro- and anti-inflammatory processes is a crucial aspect of neural defense mechanisms.

The PVT has been implicated in various functions, including stress adaptation[57,58], addictive behaviors[59,60], reward processing[61,62], and mood regulation[63,64]. Dysfunctions of the PVT are associated with various neurological abnormalities, such as anxiety[65] and depression[66]. Recently, accumulating evidence has suggested neural and functional associations between the PVT and sleep-wake regulation[7,8,67,68]. PVT neurons exhibit increased and decreased cFos expression during wakefulness and sleeping, respectively[7]. However, the role of the PVT in inflammation-induced sleepiness remains unclear. The present study quantified $cFos^+$ cells in multiple sleep-wake regulating nuclei, i.e., the PVT, BF, PVH, and VLPO, and found a significant reduction in the number of $cFos^+$ cells in the PVT after LPS injection. In vivo fiber optic recordings further confirmed that neuronal activity in the PVT was temporarily suppressed after LPS injection. Because the PVT is located on the midline just ventral to the third ventricle, where the blood–brain barrier is incomplete[12–14], PVT neurons are more vulnerable to inflammatory attacks, making them a major cause of inflammation-induced sleepiness.

Our analysis of bulk RNA-seq and scRNA-seq dataset revealed that the mRNA expression of *Hcrtr2* (encoding the OX2R) in neurons was reduced following LPS administration, and this result was confirmed by qPCR (Supplementary Fig. 2 and Fig. 4H). We hypothesize that inflammatory factors released during the inflammatory response may decrease the expression of OX2R in PVT neurons[24,69,70]. Orexin, a neuropeptide that regulates sleep/wakefulness[71], is synthesized by neurons located in the lateral hypothalamus[72,73]. These orexinergic neurons project extensively throughout the brain, particularly the PVT[8,74]. Two G protein-coupled receptors, the orexin receptor 1 (OX1R) and OX2R, have been identified as specific targets for orexin[25]. Previous research has demonstrated that OX2R are important for maintaining wakefulness. For example, OX2R knockout mice exhibit narcolepsy-like phenotypes[27,28], and the administration of an OX2R agonist can enhance wakefulness in mice[29]. OX2R pathway may mediate the reduction in neuronal activity in the PVT associated with neuroinflammation and the subsequent sleepiness.

Microglia express an array of toll-like receptors (TLRs), responsible for recognizing both invading pathogens and endogenous harmful stimuli,

thereby initiating innate and adaptive immune responses[75–77]. Among TLRs, TLR4 is the major LPS receptor[78,79]. TLR4 forms a complex with the co-receptor myeloid differentiation protein-2 (MD-2) on the cellular membrane[80,81]. Upon binding to LPS, the TLR4–MD-2 complex undergoes dimerization[82], subsequently activating downstream mediators such as the transcription factor nuclear factor-κB, increasing the production of various pro-inflammatory molecules, including TNF-α, IL-1β, IL-16, chemokines, reactive oxygen and nitrogen species[83,84]. On one hand, these molecules recruit additional cells and facilitate the clearance of pathological agents[56,85]. On the other hand, an excessive inflammatory response can have detrimental effects on neurons, which is a major cause of neurodegenerative disorders[85]. Therefore, a balance between pro- and anti-inflammatory processes needs to be maintained during neuroinflammation. Our results revealed that, on day 1 after LPS injection, microglia in the PVT were activated, accompanied by an upregulated expression of genes associated with the response to biotic stimulus, inflammatory response, and cytokine-mediated signaling pathways. In contrast, the expression of genes related to locomotion, rhythm, and neuron-related processes was downregulated. However, on day 7, microglial activation was reduced, and the transcriptome changes in the PVT were reversed. The reason how the state of microglia was restored and the pro-inflammatory response was suppressed remains unclear. Among the genes in the microglia upregulated by LPS, we found that Acod1 might play an important role in inhibiting neuroinflammation and protecting neuronal functions. We first confirmed that the level of Acod1 protein expression in the PVT coincided with microglial activation. Then, after knockdown of the expression of Acod1 in PVT microglia, we found that the inflammatory response, neuronal hypoactivation, and sleepiness were exacerbated.

Acod1, also known as immune responsive gene 1, was originally identified as a gene highly induced by LPS in mouse macrophages[86]. It encodes a crucial mitochondrial enzyme in the tricarboxylic acid cycle, which catalyzes cis-aconitate to produce itaconate[87,88]. Itaconate has been shown to limit inflammation by inhibiting succinate dehydrogenase, an important pro-inflammatory regulator[37]. Additionally, endogenous itaconate can activate the anti-inflammatory response mediated by nuclear factor erythroid 2-related factor 2 through the alkylation of Kelch-like ECH-associated protein 1[36]. Furthermore, itaconate restricts the production of pro-inflammatory cytokines by increasing the expression of activating transcription factor 3, which acts as a negative regulator of nuclear factor-κB[89,90]. In a recent study, global knockout of Acod1 significantly increased the volume of lesions in a mouse model of cerebral ischemia-reperfusion injury[91]. Another study revealed that Acod1 was induced in microglia following ischemic stroke, and Acod1 knockout mice displayed reduced expression of microglial HO-1 and exacerbated ischemic brain injury[92]. To date, the role of Acod1 in microglia has not been comprehensively investigated. In the present study, we specifically manipulated the expression of Acod1 gene in PVT microglia via stereotactic injection of adenovirus. Consistent with previous reports[93,94], our results confirmed that Acod1 exerted anti-inflammatory effects in microglia.

Exogenous supplementation of synthesized itaconate derivatives is another approach to investigate the immunomodulatory function of itaconate[95]. In comparison to endogenous itaconate, itaconate derivatives, such as dimethyl itaconate (DI) and 4-OI, exhibit lower polarity and better cell permeability, enabling them to cross the blood-brain barrier as cellular permeates with greater ease[96]. A previous study has demonstrated that DI can ameliorate disease severity in a chronic experimental autoimmune encephalomyelitis mouse model by suppressing microglial activation and the CNS infiltration of Th1 and Th17 cells[97]. However, analysis of itaconate uptake and metabolism indicated that DI was not metabolized into itaconate in mouse macrophages[98]. In contrast, 4-OI poses thiol reactivity similar to itaconate and can be hydrolyzed to itaconate by esterases in LPS-activated macrophages[36,95]. Moreover, a recent study showed that 4-OI significantly alleviated cognitive dysfunction and hippocampal neurogenesis impairment in rats exposed to β2-microglobulin[99]. Our study found that supplementation of 4-OI effectively reduced the activation of PVT microglia and the levels of pro-inflammatory cytokines in LPS-treated mice. Consequently, neuronal hypoactivation and sleepiness were improved. Therefore, 4-OI has therapeutic potential as a neuroprotective agent against neuroinflammation.

We also examined the molecular mechanisms underlying the anti-inflammatory effects of itaconate in BV2 microglia. Our findings corroborate previous research on macrophages[95,100,101], where administration 4-OI, as a pretreatment prior to LPS exposure, effectively ameliorated the dysregulation in the Keap1/Nrf2/HO-1/HIF-1α signaling axis. Moreover, the HO-1 inhibitor ZnPP partially reversed the 4-OI-indcued upregulation of HO-1 expression and restored the levels of HIF-1α in BV2 cells challenged with LPS. Additionally, ZnPP diminished the inhibitory effects of 4-OI on mitochondrial $H_2O_2$ generation and the expression of IL-1β in LPS-stimulated BV2 cells. These findings collectively imply that 4-OI may exert an inhibitory effect on microglial activation by modulating the Keap1/Nrf2/HO-1/HIF-1α signaling cascade, thereby ameliorating neuronal activity dysfunction and alleviate symptoms of sleepiness associated with neuroinflammation.

However, it is imperative to recognize that itaconate's role in biological systems is not uniformly beneficial. For example, itaconate is among the metabolites produced by pro-inflammatory subtypes of tumor-associated macrophages, potentially contributing to tumorigenesis[102]. Additionally, itaconate has been shown to competitively inhibit erythroid-specific 5-aminolevulinate synthase, which is the initial and rate-limiting step in heme synthesis. This inhibition can disrupt erythropoietic heme synthesis, leading to anemia during inflammatory episodes within the erythroid lineage[103]. For the clinical translation of itaconate, these potential adverse effects warrant vigilant attention and necessitate further investigation to fully elucidate the safety profile and therapeutic index of this promising compound.

In the interpretation of our results, it is necessary fully consider the limitations of our study. Sleepiness is a multifaceted phenomenon that is intricately linked with neuroinflammation. While LPS administration has been conventionally employed as a model to emulate neuroinflammation, the model is a transient inflammatory response with a rapid onset and a pronounced magnitude, which may not accurately reflect the chronic and varied nature of neuroinflammation. Additionally, the LPS model predominantly targets the TLR4 pathway, potentially overlooking the diversity of inflammatory pathways that contribute to the pathogenesis of sleepiness. Future research endeavors should apply more comprehensive models to verify the validity and generalizability of our findings in the context of inflammation-induced sleep disorders.

In conclusion, we observed that LPS-treated mice, as a mouse model of neuroinflammation, exhibited temporary sleepiness lasting for 7 days, accompanied by microglial activation and neuronal hypoactivation in the PVT. Moreover, Acod1 in the microglia played an anti-inflammatory and neuroprotective role during LPS-induced neuroinflammation. Exogenous supplementation of 4-OI could inhibit microglial activation and relieve neuronal dysfunction. Our findings shed light on the role of PVT in inflammation-induced sleepiness and suggest that Acod1 might be a potential therapeutic target for neuroinflammation.

## Methods

### Animals

Male and female C57BL/6 wild-type mice aged 8–12 weeks were obtained from the Department of Laboratory Animal Science of China Medical University. $Fos^{2A\text{-}iCreER}$ (TRAP2) mice (RRID: IMSR_JAX: 030323) and B6.Cg-Gt(ROSA)26Sor$^{tm14(CAG\text{-}tdTomato)Hze}$/J (Ai14) mice (RRID: IMSR_JAX: 007914) were obtained from the Jackson Laboratory. The mice were housed under standard conditions, which included a 12-h light and 12-h dark cycle, and a temperature range of 18–22 °C. The mice were kept in conventional laboratory cages with ad libitum access to food and water. All animal

experimental protocols were approved by the Animal Ethics Committee of China Medical University in accordance with Institutional Animal Care and Use Committee guidelines for animal research. We have complied with all relevant ethical regulations for animal use.

### Endotoxin-induced model of neuroinflammation

Mice were intraperitoneally injected with a single dose of LPS (1 mg/kg, Cat# L5024; Sigma, St. Louis, MO, USA) at ZT 12:00. Control mice received an equivalent volume of PBS. For the administration of 4-OI, mice were intraperitoneally injected with 4-OI (25 mg/kg, Cat# HY-112675, MCE, Monmouth Junction, NJ, USA) dissolved in 40% cyclodextrin in PBS or received the vehicle 2 h before, 12 h after, and 24 h after LPS injection.

### Electrode implantation

The mice were anesthetized with 3% isoflurane in air for induction and maintained with 1.5%. To reduce brain edema and the viscosity of bronchial secretions, dexamethasone (0.25 mg/kg) and atropine sulfate (0.1 mg/kg) were administered intraperitoneally at the beginning and end of surgery, respectively. Stainless steel screw electrodes were implanted in the PFC of the mice, following coordinates based on a mouse brain atlas (The Mouse Brain in Stereotaxic Coordinates, 3rd Edition; anteroposterior = +1.8 mm, mediolateral = ±0.5 mm, dorsoventral = –2.5 mm). A silver microwire electrode (A-M Systems, Sequim, WA, USA) was used, with one end fixed to the bone with the screws and the other end soldered to a pin connector secured to the skull with dental cement. Additionally, two stainless steel screw electrodes were placed over the cerebellum as the ground, and two additional skull screws were implanted as anchors. The mice were allowed 1 week for recovery before further experimentation.

### Electrophysiological recordings and analysis

At ZT 12:00, the mice underwent a 12-h acclimation period of head fixation and familiarization with the environment. During this period, they were allowed to move freely in place on a spinning disk. This procedure was repeated for 3 days, and recording experiments bagan on day 4. EEG signals were acquired using a flexible, low-noise cable connected to the implanted skull connector. The microwire output was delivered to a multichannel preamplifier (PBX Preamplifier; Plexon, Dallas, TX, USA) and then to a digital multichannel acquisition processor (Plexon). The EEG waveforms were amplified, low-pass filtered with a cutoff frequency of 300 Hz, and analyzed in the MATLAB environment (MATLAB R2018a; MathWorks, Natick, MA, USA).

The EEG data were categorized into wake, NREM, and REM episodes using a heuristic automated approach combined with independent visual classification[21]. First, spectrograms were computed using the recorded EEG signals, and PCA was conducted on each spectrogram. The first principal component (PC1) represented power in the low-frequency range, with the weights of frequencies < 25 Hz being opposite in sign to those of frequencies in the gamma range. By analyzing the bimodal distribution of PC1 magnitude, a threshold was determined at the trough between the two peaks, enabling the classification of each second as NREM (high PC1 power) or "other" (low PC1 power). Subsequently, the "other" epochs were further classified based on a narrow-band theta power ratio (5–10 Hz/2–16 Hz) and electromyogram (EMG) measures. Epochs exhibiting high theta power and low EMG activity were designated as REM. The remaining epochs were categorized as wake episodes.

### Tamoxifen induction

TRAP2 mice were crossed with Ai14 mice to generate the double heterozygous (TRAP2;Ai14) mice. The preparation of 4-hydroxytamoxifen (4-OHT, Cat# H6278; Sigma) solutions followed previously described methods[104]. Briefly, 4-OHT was dissolved in ethanol at a concentration of 20 mg/mL by shaking at 37 °C for 15 min and was then aliquoted and stored at −20 °C. Prior to use, the 4-OHT was redissolved in ethanol by shaking at 37 °C for 15 min. A 1:4 mixture of castor oil:sunflower seed oil (Cat# 259853 and S5007; Sigma) was added to achieve a final concentration of 10 mg/mL 4-OHT. The ethanol was evaporated by vacuum under centrifugation. The final 10 mg/mL 4-OHT solutions were used on the day they were prepared. All 4-OHT injections (50 mg/kg) were delivered intraperitoneally 1 day after PBS/LPS injection, and 7 days after LPS injection. Mice were sacrificed for further experiments 4 days after the 4-OHT administration.

### Immunofluorescence staining

Mice were anesthetized with isoflurane and transcardially perfused with saline, followed by 4% paraformaldehyde. The entire brain was then removed and immersed in 4% paraformaldehyde at 4 °C for 24 h and subsequently transferred to 30% sucrose for another 72 h. Frozen sections with a thickness of 15 μm were obtained using a cryostat (CM 1950; Leica, Wetzlar, Germany). For Fos imaging, TRAP2;Ai14 mice were used. Sections from the PVT, BF, PVH, and VLPO were stained with DAPI (Cat# D3571; Invitrogen, Waltham, MA, USA). To visualize neurons, astrocytes, and microglia, sections were incubated overnight at 4 °C with primary antibodies against neuronal nuclear antigen (NeuN, 1:500, Cat# ab177487; Abcam, Cambridge, UK), glial fibrillary acidic protein (GFAP, 1:500, Cat# ab7260; Abcam), or ionized calcium-binding adapter molecule 1 (Iba1, 1:100, Cat# ab283319 and ab178846; Abcam). For Acod1 staining, sections were immunostained with a primary antibody against Acod1 (1:50, Cat# TA372525S; OriGene, Wuxi, China). Following primary antibody incubation, the sections were incubated with a fluorescently tagged secondary antibody (1:200, Cat# SA00013-1, SA00013-2, and SA00013-4; Proteintech, Rosemont, IL, USA) at room temperature for 1 h. Subsequently, these sections were examined under a fluorescence microscope (NE910; Nexcope, Ningbo, China). Immunonegative regions were manually identified and quantified using ImageJ software (NIH, Bethesda, MD, USA).

### Fiber photometry recording

AAV carrying the calcium indicator GCaMP6 under the control of calmodulin kinase II promoter (AAV-CaMKII-GCaMP6, BrainVTA, Wuhan, China) was used. And 0.3 μl AAV-CaMKII-GCaMP6 was stereotaxically injected into the PVT (anteroposterior = −1.3 mm, mediolateral = +0.05 mm, dorsoventral = −2.8 mm) using a glass pipette microinjector and a microsyringe pump controller (RWD Life Science, San Diego, CA, USA). After the injection, the glass pipette was left in place for 5 min to prevent backflow. Subsequently, a fiber optic cannula with a ceramic ferrule (Newdoon, Hangzhou, China) was mounted to a stereotaxic cannula holder and implanted 0.2 mm above the injection site. Dental cement was employed to secure the fiber cannula to the skull. The fiber photometry recordings were conducted 3 weeks after the implantation. For fiber photometry data processing, we derived the value of the photometry signal F as F470/F410, calculating $\Delta F/F = (F - F0) / F0$, where F0 is the median of the photometry signal. A calcium transient event was defined as a change at least one standard deviation above the mean value of $\Delta F/F$.

### Bulk RNA sequencing analysis

On day 1 after PBS/LPS injection or day 7 after LPS injection, mice were anesthetized and sacrificed, and fresh PVT tissues were collected. Total RNA was extracted using the Trizol Reagent. The concentration, quality, and integrity of the extracted RNA were evaluated using a NanoDrop spectrophotometer (Thermo Scientific, Wilmington, DE, USA). Subsequently, sequencing libraries were generated using the TruSeq RNA Sample Preparation Kit (Illumina, San Diego, CA, USA). The library fragments were purified using the AMPure XP system (Beckman Coulter, Beverly, MA, USA) to select cDNA fragments with a desired length of 200 bp. The DNA fragments, which had adaptor molecules ligated on both ends, were selectively enriched using the Illumina PCR Primer Cocktail after 15 cycles of PCR reaction. Following purification, the products were quantified using the Agilent high-sensitivity DNA assay on a Bioanalyzer 2100 system (Agilent, Santa Clara, CA, USA). The sequencing library was then subjected to sequencing on a Novaseq PE150 System (Illumina) and performed by Shanghai Personal

Biotechnology Cp. Ltd (Shanghai, China). The filtered Reads were aligned to the reference genome using the upgrade version of TopHat2, HISAT2 software, with the objective of achieving a sequence mapping rate exceeding 90%. The reads were uniformly distributed across all expressed genes. HTSeq was used to statistically compare the read count value of each gene, as the original expression amount of the gene.

PCA plots were generated with the variance-stabilizing transformation normalization of the DESeq2 R package. DEGs were identified using the DESeq2 package, with an adjusted $P$-value < 0.01, $\log_2$ (fold change) > 1 used as the criteria for differential expression. Volcano plots of the DEGs were visualized using the ggplot2 R package. The gene expression heatmap was generated using the pheatmap R package. GO enrichment analysis, including BPs, was performed using the clusterProfiler R package.

### qPCR

Total RNA was extracted from PVT tissues using TRIzol reagent (Invitrogen, Camarillo, CA, USA), and first-strand cDNAs were synthesized using the PrimeScript RT reagent kit (Cat# RR047A; TaKaRa, Shiga, Japan). qPCR was performed using SYBR Premix Ex Taq (Cat# RR390A; TaKaRa) and the QuantStudio 6 RT-PCR system (ABI, Waltham, MA, USA). The $2^{-\Delta\Delta Ct}$ formula was used to calculate the relative amounts of transcripts[105], which were normalized to GAPDH as an internal control. The primers are provided in Supplementary Table 1.

### scRNA-seq datasets analysis

We downloaded three scRNA-seq datasets (accession numbers: GSE112436, GSE115571, and GSE157480) from the Gene Expression Omnibus. These datasets contained single-cell transcriptomes derived from the mouse brain after acute treatment with LPS. To identify the DEGs in neurons, astrocytes, and microglia, we used the FindMarker function in the Seurat R package and the Wilcoxon rank-sum test, taking an adjusted $P$-value < 0.01 and $\log_2$ (fold change) > 0.25 as the criteria for differential expression. Venn diagrams were generated using the Venn Diagram package in R.

### Cell culture and treatments

Mouse microglial cell line BV2 were cultured in Dulbecco's modified Eagle's medium (DMEM, Cat# PM150210, Pricella, Wuhan, China) supplemented with 10% fetal bovine serum (FBS, Cat# FBS01, Sino Biological, Beijing, China), 100 U/ml penicillin and 100 μg/ml streptomycin in a humidified 95% air-5% $CO_2$ incubator at 37°C. When reaching 60% to 70% confluence, the BV2 cells were exposed to LPS (1.0 μg/ml) for a designed time point. To examine the effect of 4-OI, 4-OI was added 2 hours before LPS treatment. Then the cells were treated by LPS for 12 hours. To determine the effect of the HO-1 inhibitor, ZnPP (10 μM, Cat# HY-101193, MCE) was added together with 4-OI. Furthermore, cells were transfected with a rLV-CMV-mito-HyPer7 (Cat# LV-0808, BrainVTA, Wuhan, China) using a Liposomal Transfection Reagent (Cat# 40802ES01, Yeasen, Shanghai, China) according to the manufacturer's instructions.

### Western blot

Total protein lysates were extracted from the PVT tissue or BV2 cells. An equal amount of proteins (30 μg per lane) were separated by electrophoresis on 8% or 10% polyacrylamide gels and transferred onto polyvinylidene difluoride membranes (EMD Millipore, Burlington, MA, USA). The membranes were then incubated with primary antibodies against Acod1 (1:500, Cat# TA372525S; OriGene), Keap1(1:2000, Cat# 10503-2-AP; Proteintech), Nrf2 (1:2000, Cat#16396-1-AP; Proteintech), HO-1 (1:1000, Cat# HA721854; HuaAn, Hangzhou, China), HIF-1α (1:1000, Cat# ab179483, Abcam), and β-actin (1:1,000, Cat# sc-8432; Santa Cruz Biotechnology, Dallas, TX, USA). Horseradish peroxidase-conjugated anti-IgG secondary antibodies were applied (1:5,000, Cat# ZB-2301 and ZB-2305; ZSGB-BIO, Beijing, China). The relative amount of proteins in each band was quantified using ImageJ (NIH) and normalized to β-actin as an internal loading control.

### Expression systems and stereotactic injection

Knockdown of Acod1 in the PVT microglia was performed by stereotactic injection of shRNA AAV. AAV-Cx3cr1-Acod1-shRNA-EGFP, and its control AAV-Cx3cr1-shRNA-EGFP were designed and constructed by standard methods. The sequence of shRNA targeting Acod1 was 5'-GCA CAGAAGTGTTCCATAAAG-3'[106]. Intracranial viral injections were performed by targeting 0.3 μl of viral vectors to the PVT. Subsequent experiments were conducted 3 weeks after the injections.

### IL-1β assay

IL-1β in culture supernatant of BV2 cells were analyzed by ELISA kits (Cat# EK201B, MULTI SCIENCES, Hangzhou, China) according to the manufacturer's instructions.

### Statistics and reproducibility

All experiments were designed to ensure robust statistical analysis and reproducibility. Statistical analysis was performed using the Origin software (OriginLab, Northampton, MA, USA), and the data are presented as mean ± standard error. To test for normality and homoscedasticity, the Shapiro-Wilk and Levene tests were conducted, respectively. For comparisons between multiple groups on one factor in independent samples, one-way analysis of variance (ANOVA) followed by Tukey's test was performed for parametric data, and the Kruskal-Wallis test followed by Dunn's test was performed for non-parametric data. In the case of repeated measures, comparisons between multiple groups on one factor were conducted using one-way repeated-measures ANOVA followed by Tukey's test for parametric data, and Friedman's ANOVA followed by Dunn's test was employed for non-parametric data. When comparing multiple groups involving two factors, two-way ANOVA followed by Tukey's test was used for independent samples, and two-way repeated-measures ANOVA followed by Tukey's test were employed for repeated measures. Statistical significance was defined as a $P$-value < 0.05.

To assess the reproducibility of our experiments, we paid close attention to sample sizes and the number of replicates. Each experiment was repeated at least three times to confirm reproducibility, with the specific number of replicates detailed in the figure legends. Replicates were defined as independent experimental trials conducted under identical conditions. For experiments involving animal models, we ensured that each replicate was performed with a separate group of animals to avoid biases from individual variability. For in vitro experiments, each replicate was derived from a separate cell preparation or passage to ensure consistency and reproducibility.

### Reporting summary

Further information on research design is available in the Nature Portfolio Reporting Summary linked to this article.

## Data availability

RNA-seq data have been archived in the Gene Expression Omnibus repository under the accession number GSE280081. Source data underlying analyses for plots and graphs are detailed in Supplementary Data 1. Images of uncropped and unedited western blots are provided in Supplementary Fig. 3. Additionalinformation is available from the corresponding author upon reasonable request.

## Code availability

The custom codes used for analyzing data are available at https://github.com/Jianjun1992/Jianjun

Received: 26 March 2024; Accepted: 5 November 2024;
Published online: 10 November 2024

## References

1. Navarro, E., Norden, D. M., Trojanowski, P. J., Godbout, J. P. & López, M. G. Central activation of alpha7 nicotinic signaling

attenuates LPS-induced neuroinflammation and sickness behavior in adult butnot in aged animals. *Molecules.* **26**, 2107 (2021).
2. Bever, S. R., Liu, X., Quan, N. & Pyter, L. M. Euflammation attenuates central and peripheral inflammation and cognitive consequences of an immune challenge after tumor development. *Neuroimmunomodulation.* **24**, 74–86 (2017).
3. Siciliano, V. et al. Viral encephalitis in adults: a narrative review. *Rev Recent Clin Trials.* **17**, 259–267 (2022).
4. Ferrari-Marinho, T., De Marchi, L. R. & Caboclo, L. O. Clinical neurophysiology of zika virus encephalitis. *J Clin Neurophysiol.* **39**, 259–264 (2022).
5. Tesoriero, C., Del Gallo, F. & Bentivoglio, M. Sleep and brain infections. *Brain Res Bull.* **145**, 59–74 (2019).
6. Saper, C. B., Romanovsky, A. A. & Scammell, T. E. Neural circuitry engaged by prostaglandins during the sickness syndrome. *Nat Neurosci* **15**, 1088–1095 (2012).
7. Ren, S. et al. The paraventricular thalamus is a critical thalamic area for wakefulness. *Science.* **362**, 429–434 (2018).
8. Colavito, V., Tesoriero, C., Wirtu, A. T., Grassi-Zucconi, G. & Bentivoglio, M. Limbic thalamus and state-dependent behavior: The paraventricular nucleus of the thalamic midline as a node in circadian timing and sleep/wake-regulatory networks. *Neurosci Biobehav Rev.* **54**, 3–17 (2015).
9. Chen, C. et al. Adenosine downregulates the activities of glutamatergic neurons in the paraventricular hypothalamic nucleus required for sleep. *Front Neurosci.* **16**, 907155 (2022).
10. Peng, W. et al. Regulation of sleep homeostasis mediator adenosine by basal forebrain glutamatergic neurons. *Science.* **369**, eabb0556 (2020).
11. Kroeger, D. et al. Galanin neurons in the ventrolateral preoptic area promote sleep and heat loss in mice. *Nat Commun.* **9**, 4129 (2018).
12. Van der Werf, Y. D., Witter, M. P. & Groenewegen, H. J. The intralaminar and midline nuclei of the thalamus. Anatomical and functional evidence for participation in processes of arousal and awareness. *Brain Res Brain Res Rev.* **39**, 107–140 (2002).
13. Smith, Y., Raju, D. V., Pare, J. F. & Sidibe, M. The thalamostriatal system: a highly specific network of the basal ganglia circuitry. *Trends Neurosci.* **27**, 520–527 (2004).
14. Rijnsburger, M., Unmehopa, U. A., Eggels, L., Serlie, M. J. & la Fleur, S. E. One-week exposure to a free-choice high-fat high-sugar diet does not disrupt blood-brain barrier permeability in fed or overnight fasted rats. *Nutr Neurosci.* **22**, 541–550 (2019).
15. Miyamoto, A. et al. Microglia contact induces synapse formation in developing somatosensory cortex. *Nat Commun.* **7**, 12540 (2016).
16. Park, T., Chen, H. & Kim, H. Y. GPR110 (ADGRF1) mediates anti-inflammatory effects of N-docosahexaenoylethanolamine. *J Neuroinflammation.* **16**, 225 (2019).
17. Bray, C. E. et al. Chronic cortical inflammation, cognitive impairment, and immune reactivity associated with diffuse brain injury are ameliorated by forced turnover of microglia. *J Neurosci.* **42**, 4215–4228 (2022).
18. Chen, N. C., Partridge, A. T., Sell, C., Torres, C. & Martín-García, J. Fate of microglia during HIV-1 infection: From activation to senescence? *Glia.* **65**, 431–446 (2017).
19. Rock, R. B. & Peterson, P. K. Microglia as a pharmacological target in infectious and inflammatory diseases of the brain. *J Neuroimmune Pharmacol.* **1**, 117–126 (2006).
20. Zhao, G. et al. Toll-like receptor 2 signaling pathway activation contributes to a highly efficient inflammatory response in Japanese encephalitis virus-infected mouse microglial cells by proteomics. *Front Microbiol.* **13**, 989183 (2022).
21. Watson, B. O., Levenstein, D., Greene, J. P., Gelinas, J. N. & Buzsáki, G. Network homeostasis and state dynamics of neocortical sleep. *Neuron.* **90**, 839–852 (2016).
22. Chen, C. R. et al. Dysfunctions of the paraventricular hypothalamic nucleus induce hypersomnia in mice. *eLife.* **10**, e69909 (2021).
23. Duan, L. et al. PDGFRβ cells rapidly relay inflammatory signal from the circulatory system to neurons via chemokine CCL2. *Neuron.* **100**, 183–200.e8 (2018).
24. Zhan, S. et al. Tumor necrosis factor-alpha regulates the hypocretin system via mRNA degradation and ubiquitination. *Biochim Biophys Acta.* **1812**, 565–571 (2011).
25. Sakurai, T. et al. Orexins and orexin receptors: a family of hypothalamic neuropeptides and G protein-coupled receptors that regulate feeding behavior. *Cell.* **92**, 573–585 (1998).
26. Clark, I. A. & Vissel, B. Inflammation-sleep interface in brain disease: TNF, insulin, orexin. *J Neuroinflammation.* **11**, 51 (2014).
27. Willie, J. T., Chemelli, R. M., Sinton, C. M. & Yanagisawa, M. To eat or to sleep? Orexin in the regulation of feeding and wakefulness. *Annu Rev Neurosci.* **24**, 429–458 (2001).
28. Sakurai, T. The neural circuit of orexin (hypocretin): maintaining sleep and wakefulness. *Nat Rev Neurosci.* **8**, 171–181 (2007).
29. Ishikawa, T. et al. TAK-994, a novel orally available bbrain-penetrant orexin 2 receptor-selective agonist, suppresses fragmentation of wakefulness and cataplexy-like episodes in mouse models of narcolepsy. *J Pharmacol Exp Ther* **385**, 193–204 (2023).
30. Sousa, C. et al. Single-cell transcriptomics reveals distinct inflammation-induced microglia signatures. *EMBO Rep.* **19**, e46171 (2018).
31. Shemer, A. et al. Interleukin-10 prevents pathological microglia hyperactivation following peripheral endotoxin challenge. *Immunity.* **53**, 1033–1049.e7 (2020).
32. Preissler, J. et al. Altered microglial phagocytosis in GPR34-deficient mice. *Glia.* **63**, 206–215 (2015).
33. Gómez Morillas, A., Besson, V. C. & Lerouet, D. Microglia and neuroinflammation: what place for P2RY12? *Int J Mol Sci.* **22**, 1636 (2021).
34. Chen, Z. et al. Lipopolysaccharide-induced microglial activation and neuroprotection against experimental brain injury is independent of hematogenous TLR4. *J Neurosci.* **32**, 11706–11715 (2012).
35. Zhang, J. et al. LPS activates neuroinflammatory pathways to induce depression in Parkinson's disease-like condition. *Front Pharmacol.* **13**, 961817 (2022).
36. Mills, E. L. et al. Itaconate is an anti-inflammatory metabolite that activates Nrf2 via alkylation of KEAP1. *Nature.* **556**, 113–117 (2018).
37. Mills, E. L. et al. Succinate dehydrogenase supports metabolic repurposing of mitochondria to drive inflammatory macrophages. *Cell.* **167**, 457–470.e13 (2016).
38. Kobayashi, E. H. et al. Nrf2 suppresses macrophage inflammatory response by blocking proinflammatory cytokine transcription. *Nat Commun.* **7**, 11624 (2016).
39. Pak, V. V. et al. Ultrasensitive genetically encoded indicator for hydrogen peroxide identifies roles for the oxidant in cell migration and mitochondrial function. *Cell Metab* **31**, 642–653.e646 (2020).
40. Driesse, M. J. et al. Intra-CSF administered recombinant adenovirus causes an immune response-mediated toxicity. *Gene Ther.* **7**, 1401–1409 (2000).
41. Liptai, Z. et al. Mild encephalitis/encephalopathy with a reversible splenial lesion in children. *Ideggyogy Sz.* **66**, 67–71 (2013).
42. Angus, D. C. & van der Poll, T. Severe sepsis and septic shock. *N Engl J Med.* **369**, 840–851 (2013).
43. Kim, S. M. et al. Fecal microbiota transplant rescues mice from human pathogen mediated sepsis by restoring systemic immunity. *Nat Commun.* **11**, 2354 (2020).
44. Nemzek, J. A., Hugunin, K. M. & Opp, M. R. Modeling sepsis in the laboratory: merging sound science with animal well-being. *Comp Med.* **58**, 120–128 (2008).
45. Fink, M. P. Animal models of sepsis. *Virulence.* **5**, 143–153 (2014).

46. Männel, D. N. Advances in sepsis research derived from animal models. *Int J Med Microbiol.* **297**, 393–400 (2007).
47. Silverman, M. N. et al. Glucocorticoid receptor dimerization is required for proper recovery of LPS-induced inflammation, sickness behavior and metabolism in mice. *Mol Psychiatry.* **18**, 1006–1017 (2013).
48. Frenois, F. et al. Lipopolysaccharide induces delayed FosB/DeltaFosB immunostaining within the mouse extended amygdala, hippocampus and hypothalamus, that parallel the expression of depressive-like behavior. *Psychoneuroendocrinology* **32**, 516–531 (2007).
49. André, C. et al. Spatio-temporal differences in the profile of murine brain expression of proinflammatory cytokines and indoleamine 2,3-dioxygenase in response to peripheral lipopolysaccharide administration. *J Neuroimmunol.* **200**, 90–99 (2008).
50. Ahamed, J. et al. Regulation of macrophage procoagulant responses by the tissue factor cytoplasmic domain in endotoxemia. *Blood.* **109**, 5251–5259 (2007).
51. Sheng, B. et al. Antifungal treatment aggravates sepsis through the elimination of intestinal fungi. *Oxid Med Cell Longev.* **2021**, 2796700 (2021).
52. Ren, X. et al. Macrophage-endothelial cell crosstalk orchestrates neutrophil recruitment in inflamed mucosa. *J Clin Invest.* **133**, e170733 (2023).
53. Min, B. K., Suk, K. & Lee, W. H. Stimulation of CD107 affects LPS-induced cytokine secretion and cellular adhesion through the ERK signaling pathway in the human macrophage-like cell line, THP-1. *Cell Immunol.* **281**, 122–128 (2013).
54. Candelario-Jalil, E., Dijkhuizen, R. M. & Magnus, T. Neuroinflammation, stroke, blood-brain barrier dysfunction, and imaging modalities. *Stroke.* **53**, 1473–1486 (2022).
55. Denes, A. et al. Endothelial cells and macrophages as allies in the healthy and diseased brain. *Acta Neuropathol.* **147**, 38 (2024).
56. Hickman, S., Izzy, S., Sen, P., Morsett, L. & El Khoury, J. Microglia in neurodegeneration. *Nat Neurosci.* **21**, 1359–1369 (2018).
57. Hsu, D. T., Kirouac, G. J., Zubieta, J. K. & Bhatnagar, S. Contributions of the paraventricular thalamic nucleus in the regulation of stress, motivation, and mood. *Front Behav Neurosci.* **8**, 73 (2014).
58. Beas, B. S. et al. The locus coeruleus drives disinhibition in the midline thalamus via a dopaminergic mechanism. *Nat Neurosci.* **21**, 963–973 (2018).
59. James, M. H. & Dayas, C. V. What about me…? The PVT: a role for the paraventricular thalamus (PVT) in drug-seeking behavior. *Front Behav Neurosci.* **7**, 18 (2013).
60. Martin-Fardon, R. & Boutrel, B. Orexin/hypocretin (Orx/Hcrt) transmission and drug-seeking behavior: is the paraventricular nucleus of the thalamus (PVT) part of the drug seeking circuitry? *Front Behav Neurosci.* **6**, 75 (2012).
61. Ong, Z. Y., Liu, J. J., Pang, Z. P. & Grill, H. J. Paraventricular thalamic control of food intake and reward: role of glucagon-like peptide-1 receptor signaling. *Neuropsychopharmacology.* **42**, 2387–2397 (2017).
62. Do-Monte, F. H., Minier-Toribio, A., Quiñones-Laracuente, K., Medina-Colón, E. M. & Quirk, G. J. Thalamic regulation of sucrose seeking during unexpected reward omission. *Neuron.* **94**, 388–400 (2017).
63. Price, J. L. & Drevets, W. C. Neurocircuitry of mood disorders. *Neuropsychopharmacology.* **35**, 192–216 (2010).
64. Penzo, M. A. et al. The paraventricular thalamus controls a central amygdala fear circuit. *Nature.* **519**, 455–459 (2015).
65. Zhu, Y. B. *et al*. PBN-PVT projections modulate negative affective states in mice. *eLife*. **11** (2022).
66. Kasahara, T. et al. Depression-like episodes in mice harboring mtDNA deletions in paraventricular thalamus. *Mol Psychiatry.* **21**, 39–48 (2016).
67. Shao, Y. F., Lin, J. S. & Hou, Y. P. Paraventricular thalamus as a major thalamic structure for wake control. *Neurosci Bull.* **35**, 946–948 (2019).
68. Gent, T. C., Bassetti, C. & Adamantidis, A. R. Sleep-wake control and the thalamus. *Curr Opin Neurobiol.* **52**, 188–197 (2018).
69. Guo, J. et al. Therapeutic effects of orexin-A in sepsis-associated encephalopathy in mice. *J Neuroinflammation.* **21**, 131 (2024).
70. Madaan, P. et al. Exploring the Therapeutic potential of targeting purinergic and orexinergic receptors in alcoholic neuropathy. *Neurotox Res.* **40**, 646–669 (2022).
71. Tsujino, N. & Sakurai, T. Orexin/hypocretin: a neuropeptide at the interface of sleep, energy homeostasis, and reward system. *Pharmacol Rev.* **61**, 162–176 (2009).
72. Chase, M. H. A unified survival theory of the functioning of the hypocretinergic system. *J Appl Physiol (1985).* **115**, 954–971 (2013).
73. Li, J., Hu, Z. & de Lecea, L. The hypocretins/orexins: integrators of multiple physiological functions. *Br J Pharmacol.* **171**, 332–350 (2014).
74. Sutcliffe, J. G. & de Lecea, L. The hypocretins: excitatory neuromodulatory peptides for multiple homeostatic systems, including sleep and feeding. *J Neurosci Res.* **62**, 161–168 (2000).
75. Shemer, A., Erny, D., Jung, S. & Prinz, M. Microglia plasticity during health and disease: an immunological perspective. *Trends Immunol.* **36**, 614–624 (2015).
76. Arandjelovic, S. & Ravichandran, K. S. Phagocytosis of apoptotic cells in homeostasis. *Nat Immunol.* **16**, 907–917 (2015).
77. Kawai, T. & Akira, S. The role of pattern-recognition receptors in innate immunity: update on Toll-like receptors. *Nat Immunol.* **11**, 373–384 (2010).
78. Poltorak, A. et al. Defective LPS signaling in C3H/HeJ and C57BL/10ScCr mice: mutations in Tlr4 gene. *Science.* **282**, 2085–2088 (1998).
79. Park, B. S. & Lee, J. O. Recognition of lipopolysaccharide pattern by TLR4 complexes. *Exp Mol Med.* **45**, e66 (2013).
80. Shimazu, R. et al. MD-2, a molecule that confers lipopolysaccharide responsiveness on Toll-like receptor 4. *J Exp Med.* **189**, 1777–1782 (1999).
81. Ohto, U., Fukase, K., Miyake, K. & Satow, Y. Crystal structures of human MD-2 and its complex with antiendotoxic lipid IVa. *Science.* **316**, 1632–1634 (2007).
82. Park, B. S. et al. The structural basis of lipopolysaccharide recognition by the TLR4-MD-2 complex. *Nature.* **458**, 1191–1195 (2009).
83. Bryant, C. E., Spring, D. R., Gangloff, M. & Gay, N. J. The molecular basis of the host response to lipopolysaccharide. *Nat Rev Microbiol.* **8**, 8–14 (2010).
84. Zusso, M. et al. Ciprofloxacin and levofloxacin attenuate microglia inflammatory response via TLR4/NF-kB pathway. *J Neuroinflammation.* **16**, 148 (2019).
85. Glass, C. K., Saijo, K., Winner, B., Marchetto, M. C. & Gage, F. H. Mechanisms underlying inflammation in neurodegeneration. *Cell.* **140**, 918–934 (2010).
86. Lee, C. G., Jenkins, N. A., Gilbert, D. J., Copeland, N. G. & O'Brien, W. E. Cloning and analysis of gene regulation of a novel LPS-inducible cDNA. *Immunogenetics*. **41** (1995).
87. Lampropoulou, V. *et al*. Itaconate links inhibition of succinate dehydrogenase with macrophage metabolic remodeling and regulation of inflammation. *Cell Metab*. **24** (2016).
88. Michelucci, A. et al. Immune-responsive gene 1 protein links metabolism to immunity by catalyzing itaconic acid production. *Proc Natl Acad Sci USA.* **110**, 7820–7825 (2013).
89. Bambouskova, M. et al. Electrophilic properties of itaconate and derivatives regulate the IκBζ-ATF3 inflammatory axis. *Nature.* **556**, 501–504 (2018).

90. Swain, A. et al. Comparative evaluation of itaconate and its derivatives reveals divergent inflammasome and type I interferon regulation in macrophages. *Nat Metab.* **2**, 594–602 (2020).
91. Vigil, T. M., Frieler, R. A., Kilpatrick, K. L., Wang, M. M. & Mortensen, R. M. Aconitate decarboxylase 1 suppresses cerebral ischemia-reperfusion injury in mice. *Exp Neurol.* **347**, 113902 (2022).
92. Kuo, P. C. et al. Immunoresponsive gene 1 modulates the severity of brain injury in cerebral ischaemia. *Brain Commun.* **3**, fcab187 (2021).
93. Ni, L. et al. Immune-responsive gene 1/itaconate activates nuclear factor erythroid 2-related factor 2 in microglia to protect against spinal cord injury in mice. *Cell Death Dis.* **13**, 140 (2022).
94. Ren, J. et al. Dimethyl itaconate inhibits neuroinflammation to alleviate chronic pain in mice. *Neurochem Int.* **154**, 105296 (2022).
95. Li, Z., Zheng, W., Kong, W. & Zeng, T. Itaconate: a potent macrophage immunomodulator. *Inflammation.* **46**, 1177–1191 (2023).
96. Liu, R. et al. Itaconate: A promising precursor for treatment of neuroinflammation associated depression. *Biomed Pharmacother.* **167**, 115521 (2023).
97. Kuo, P. C. et al. Dimethyl itaconate, an itaconate derivative, exhibits immunomodulatory effects on neuroinflammation in experimental autoimmune encephalomyelitis. *J Neuroinflammation.* **17**, 138 (2020).
98. ElAzzouny, M. et al. Dimethyl itaconate is not metabolized into itaconate intracellularly. *J Biol Chem.* **292**, 4766–4769 (2017).
99. Zhou, G. J. et al. Itaconate alleviates β(2)-microglobulin-induced cognitive impairment by enhancing the hippocampal amino-β-carboxymuconate-semialdehyde-decarboxylase/picolinic acid pathway. *Biochem Pharmacol.* **202**, 115137 (2022).
100. He, R. et al. Itaconate inhibits ferroptosis of macrophage via Nrf2 pathways against sepsis-induced acute lung injury. *Cell Death Discov.* **8**, 43 (2022).
101. Maassen, S. et al. Itaconate promotes a wound resolving phenotype in pro-inflammatory macrophages. *Redox Biol.* **59**, 102591 (2023).
102. Scheurlen, K. M., Billeter, A. T., O'Brien, S. J. & Galandiuk, S. Metabolic dysfunction and early-onset colorectal cancer - how macrophages build the bridge. *Cancer Med.* **9**, 6679–6693 (2020).
103. Marcero, J. R. et al. The immunometabolite itaconate inhibits heme synthesis and remodels cellular metabolism in erythroid precursors. *Blood Adv.* **5**, 4831–4841 (2021).
104. DeNardo, L. A. et al. Temporal evolution of cortical ensembles promoting remote memory retrieval. *Nat Neurosci.* **22**, 460–469 (2019).
105. Schmittgen, T. D. & Livak, K. J. Analyzing real-time PCR data by the comparative C(T) method. *Nat Protoc.* **3**, 1101–1108 (2008).
106. Li, Y. et al. Blockage of citrate export prevents TCA cycle fragmentation via Irg1 inactivation. *Cell Rep.* **38**, 110391 (2022).


## Acknowledgements

We thank Michael Irvine, from Liwen Bianji (Edanz) (www.liwenbianji.cn) for editing the English text of a draft of this manuscript. The study was funded by the Chinese National Key Technology R&D Program (2021YFC2501303 to P.T.Y.), the Joint Funds of the National Natural Science Foundation of China (U22A20309 to P.T.Y.), the Department of Science and Technology of Liaoning Province (2021JH1/10400049 to L.Q.), the 'Xingliao Talent Plan' of Liaoning Province (XLYC2002094 to L.Q.), National Natural Science Foundation of China (Youth Fund, No.82301533 to X.J.W.).

## Author contributions

J.C. contributed to the acquisition, analysis, and drafting the work. Z.L. contributed analysis of data. H.Y., X.W. and J.X. contributed acquisition of data. P.Y. and L.Q. contributed conception and design of the work; revising the work critically for important intellectual content.

## Competing interests

The authors declare no competing interest.

## Additional information

**Supplementary information** The online version contains supplementary material available at https://doi.org/10.1038/s42003-024-07215-0.

**Correspondence** and requests for materials should be addressed to Pingting Yang or Ling Qin.

**Peer review information** *Communications Biology* thanks the anonymous reviewers for their contribution to the peer review of this work. Primary Handling Editor: Benjamin Bessieres.